National Technical University of Athens
School of Mechanical Engineering
Fluids Department
Parallel CFD & Optimization Unit

Uncertainty Quantification through Adjoint-Assisted Regression-Based (Arbitrary) Polynomial Chaos Expansion

Diploma Thesis

Ioannis Lyras

Advisors:

Kyriakos C. Giannakoglou, Professor NTUA

Dr. V. Asouti, Adjunct Lecturer NTUA

Athens, 2025

Acknowledgments

First and foremost, I wish to extend my deepest gratitude to my advisor, Professor Kyriakos C. Giannakoglou. His profound expertise, unwavering dedication to teaching, and continual support have been a constant source of inspiration throughout my academic journey. I consider myself extremely fortunate to have had the opportunity to work under his expert guidance on this fascinating topic.

I would also like to express my appreciation to Dr. Varvara Asouti for her invaluable advice and guidance throughout the course of this diploma thesis. Her support and encouragement have been instrumental in shaping this work, and I am grateful for her contributions.

Finally, I extend my heartfelt thanks to my family. Their unconditional love and encouragement have been the cornerstone of my success, empowering me to pursue my dreams with confidence. I dedicate this work to them and to the loving memory of my father.

National Technical University of Athens
School of Mechanical Engineering
Fluids Department
Parallel CFD & Optimization Unit

Uncertainty Quantification through Adjoint-Assisted Regression-Based (Arbitrary) Polynomial Chaos Expansion

Diploma Thesis

Ioannis Lyras

Advisors:
Kyriakos C. Giannakoglou, Professor NTUA
Dr. V. Asouti, Adjunct Lecturer NTUA

Athens, 2025

Abstract

In modern computational science and engineering, Uncertainty Quantification (UQ) plays a pivotal role in enabling reliable and robust simulations by accounting for variabilities in input parameters. This diploma thesis investigates efficient UQ methodologies, with a particular focus on the implementation and enhancement of regression-based non-intrusive Polynomial Chaos Expansion (PCE), as well as its extension to adjoint-assisted as well as arbitrary PCE (aPCE) frameworks. The aim is to significantly reduce the computational cost of UQ in complex engineering systems, such as those governed by Computational Fluid Dynamics (CFD), without compromising accuracy.

Initially, the thesis revisits and implements the foundational non-intrusive PCE (ni-PCE) method, which circumvents intrusive reformulations of governing equations and treats the computational solver as a black box. To improve the regression process in ni-PCE, the adjoint method is incorporated to exploit gradient information of the Quantity of Interest (QoI) with respect to uncertain inputs. This adjoint-assisted regression-based PCE technique forms an overdetermined system using both QoI evaluations and their sensitivities, effectively reducing the number of required CFD simulations and accelerating convergence, especially for high-dimensional problems.

Recognizing the limitations of classical PCE in handling non-standard input dis-

tributions, the thesis further develops the arbitrary Polynomial Chaos Expansion (aPCE) framework. This data-driven approach constructs a custom orthogonal polynomial basis tailored to empirical input distributions, leveraging the Mysovskikh theorem and moment-based orthogonalization to build robust bases from limited statistical information. Both 1-D and multi-dimensional aPCE formulations are explored and rigorously verified.

To model geometric variability, particularly shape imperfections in aerodynamic applications, the Karhunen-Loève Expansion (KLE) is employed. The KLE offers a compact and accurate representation of random fields such as shape deviations, enabling their integration into the UQ framework in a mathematically consistent manner.

The developed methods are systematically verified through a series of test cases, including canonical benchmark problems like the Borehole function, and real-world engineering applications such as uncertainty analysis in airfoil performance, shape imperfections, and Supersonic Business Jet (SBJ) design metrics. Results demonstrate that the adjoint-assisted and arbitrary PCE techniques yield accurate estimates of stochastic moments (mean and variance) with drastically fewer samples than traditional approaches, such as Monte Carlo Simulation.

Overall, this diploma thesis provides a comprehensive and scalable methodology for efficient and accurate UQ in engineering systems. The integration of adjoint information and empirical distribution handling extends the frontiers of polynomial chaos expansion methods, making them suitable for a broader range of real-world CFD problems.

Εθνικό Μετσόβιο Πολυτεχνείο
Σχολή Μηχανολόγων Μηχανικών
Τομέας Ρευστών
Μονάδα Παράλληλης Υπολογιστικής Ρευστοδυναμικής
& Βελτιστοποίησης

Ποσοτικοποίηση Αβεβαιότητας μέσω (Αυθαίρετου) Πολυωνυμικού Αναπτύγματος Χάους με χρήση Γραμμικής Παλινδρόμησης και της Συζυγούς Μεθόδου

Διπλωματική Εργασία

Ιωάννης Λύρας

Επιβλέποντες:
Κυριάκος Χ. Γιαννάκογλου, Καθηγητής ΕΜΠ
Δρ. Β. Ασούτη, Εντεταλμένη Διδάσκουσα ΕΜΠ

Αθήνα, 2025

Περίληψη

Στη σύγχρονη υπολογιστική μηχανική, η Ποσοτικοποίηση Αβεβαιότητας (Uncertainty Quantification - UQ) διαδραματίζει καθοριστικό ρόλο στη δημιουργία αξιόπιστων προσομοιώσεων, λαμβάνοντας υπόψη τη στοχαστικότητα των παραμέτρων εισόδου. Η διπλωματική εργασία εστιάζει στην ανάπτυξη και βελτίωση αποδοτικών μεθόδων UQ, με έμφαση στο μη-επεμβατικό Πολυωνυμικό Ανάπτυγμα Χάους (Polynomial Chaos Expansion - PCE) βασισμένο σε γραμμική παλινδρόμηση, καθώς και στην επέκτασή του με τη χρήση παραγώγων και την προσαρμοσμένη έκδοση για αυθαίρετες κατανομές (arbitrary PCE - aPCE). Στόχος είναι η σημαντική μείωση του υπολογιστικού κόστους της UQ σε συστήματα με πολλές αβέβαιες μεταβλητές, χωρίς να επηρεάζεται η ακρίβεια των αποτελεσμάτων.

Αρχικά, η εργασία αναπτύσσει και υλοποιεί το βασικό σχήμα της μη-επεμβατικής PCE (ni-PCE), το οποίο αποφεύγει την επεμβατική αναδιατύπωση των εξισώσεων του μοντέλου και αντιμετωπίζει τον υπολογιστικό επιλυτή ως «μαύρο κουτί». Για τη βελτίωση της διαδικασίας παλινδρόμησης (regression) στην ni-PCE, ενσωματώνεται η συζυγής μέθοδος (adjoint), ώστε να αξιοποιηθούν οι, με οικονομικό τρόπο, αποκτούμενες παράγωγοι της Ποσότητας Ενδιαφέροντος (Quantity of Interest - QoI) ως προς τις αβέβαιες μεταβλητές. Αυτή η τεχνική διαμορφώνει ένα υπερκαθορισμένο σύστημα εξισώσεων, μειώνοντας δραστικά τον αριθμό των απαιτούμενων προσομοιώσεων CFD

και επιταχύνοντας τη σύγκλιση, ιδιαίτερα σε προβλήματα υψηλής διάστασης.

Αναγνωρίζοντας τους περιορισμούς του κλασικού PCE στην ανάλυση μη-τυπικών κατανομών εισόδου, η εργασία αναπτύσσει περαιτέρω το πλαίσιο του αυθαίρετου Πολυωνυμικού Αναπτύγματος Χάους (aPCE). Αυτή η προσέγγιση, βασισμένη σε δεδομένα, κατασκευάζει μια προσαρμοσμένη ορθοκανονική πολυωνυμική βάση για εμπειρικές κατανομές εισόδου, αξιοποιώντας το θεώρημα του Mysovskikh και τεχνικές ορθογωνιοποίησης βασισμένες στις στοχαστικές ροπές. Αναπτύσσονται τόσο μονοδιάστατες όσο και πολυδιάστατες εκδοχές της aPCE και ελέγχονται με αυστηρά κριτήρια.

Για την περιγραφή γεωμετρικών μεταβολών, ιδιαίτερα κατασκευαστικών ατελειών σε αεροδυναμικές εφαρμογές, χρησιμοποιείται το Ανάπτυγμα Karhunen-Loève (KLE). Το KLE παρέχει μια συνοπτική και ακριβή αναπαράσταση τυχαίων πεδίων, όπως οι μορφολογικές αποκλίσεις, επιτρέποντας την ενσωμάτωσή τους στο πλαίσιο της UQ με μαθηματική συνέπεια.

Οι παραπάνω μέθοδοι αξιολογούνται συστηματικά μέσω μιας σειράς προβλημάτων, συμπεριλαμβανομένου του απλού μαθηματικού προβλήματος Borehole, καθώς και πραγματικών εφαρμογών, όπως η ποσοτικοποίηση αβεβαιοτήτων σε ροή γύρω από αεροτομή, ατέλειες σχήματος και μετρήσεις αεροδυναμικής απόδοσης σε Υπερηχητικό Αεροσκάφος (Supersonic Business Jet - SBJ). Τα αποτελέσματα δείχνουν αυτές οι τεχνικές παρέχουν ακριβείς εκτιμήσεις στατιστικών μεγεθών (μέση τιμή, διακύμανση) με πολύ λιγότερα δείγματα σε σύγκριση με τις κλασικές μεθόδους, όπως η μέθοδος Monte Carlo.

Συνοπτικά, η εργασία αυτή προσφέρει μια ολοκληρωμένη και επεκτάσιμη μεθοδολογία για αποτελεσματική και ακριβή ποσοτικοποίηση αβεβαιότητας σε μηχανικά συστήματα. Η ενσωμάτωση πληροφορίας παραγώγων και η διαχείριση εμπειρικών κατανομών διευρύνουν το πεδίο εφαρμογής των μεθόδων PCE, καθιστώντας τις κατάλληλες για ένα ευρύτερο φάσμα προβλημάτων CFD του πραγματικού κόσμου.

Nomenclature

aPCE	Arbitrary Polynomial Chaos Expansion
CFD	Computational Fluid Dynamics
CPU	Central Processing Unit
CU	Cost Unit
EFS	Equivalent Flow Solution
GQ	Gauss Quadrature
KDE	Kernel Density Estimation
KLE	Karhunen-Loève Expansion
LHS	Latin Hypercube Sampling
MCS	Monte Carlo Simulation
MDA	Multidisciplinary Analysis
MDO	Multidisciplinary Design Optimization
ni-PCE	Non-Intrusive Polynomial Chaos Expansion
NTUA	National Technical University of Athens
PCOpt	Parallel CFD & Optimization Unit
PCE	Polynomial Chaos Expansion
QoI	Quantity of Interest
RANS	Reynolds-Averaged Navier-Stokes
RHS	Right-Hand Side
SBJ	Supersonic Business Jet
SVD	Singular Value Decomposition
UQ	Uncertainty Quantification

Contents

List of Figures

List of Tables

Chapter 1

Introduction

1.1 Uncertainty Quantification

Uncertainty Quantification (UQ) is an essential discipline within computational mechanics that focuses on propagating existing input uncertainties through nonlinear systems to assess how they influence the uncertainties in the system's responses. These uncertainties can arise from various sources, including inherent variability, measurement errors, and model approximations. The system's outputs or responses are typically referred to as the Quantities of Interest (QoIs).

The practice of UQ involves a systematic approach to identifying, quantifying, and propagating uncertainties through a model. One of the fundamental techniques employed in UQ is Monte Carlo Simulation (MCS) [17]. MCS is a statistical method that relies on random sampling to compute the probabilistic distribution of the QoI. By performing a large number of simulations with varying inputs, MCS can provide an empirical approximation to the response distribution, allowing for the estimation of statistical moments such as the mean, variance, skewness, and kurtosis of uncertain responses.

Another prominent technique used in UQ is Polynomial Chaos Expansion (PCE) [12]. PCE is a spectral method that represents the QoI as a series of orthogonal polynomials in terms of the input uncertainties [6]. This method is particularly advantageous for its efficiency in capturing the behavior of complex models with fewer simulations compared to traditional MCS. The coefficients of the expansion can be determined by either projecting the QoI onto the orthogonal polynomials (Galerkin Projection) that are numerically integrated or using regression methods.

The application of UQ spans numerous fields, including engineering, finance and environmental science. In this diploma thesis, the focus is on the application of UQ

to Computational Fluid Dynamics (CFD) simulations and optimization problems. Overall, UQ serves as a critical tool for advancing the accuracy and credibility of computational models, ultimately leading to more informed and confident decisions in the presence of uncertainty.

1.1.1 Non - Intrusive PCE

Non-Intrusive PCE (ni-PCE) [5] is a variant of PCE that does not require modifications to the existing computational model. Unlike intrusive methods that necessitate direct integration of the PCE framework into the model equations, ni-PCE treats the model as a black box within the UQ framework. This flexibility makes ni-PCE particularly appealing for complex systems where modifying the model is impractical.

Typical methods for ni-PCE include the use of quadrature, collocation, and regression techniques to determine the coefficients of the polynomial expansion. Quadrature methods involve evaluating the model at specific input points and integrating numerically, while collocation methods use a predefined set of sample points to construct the polynomial basis.

A prominent approach within the ni-PCE is regression-based PCE, which leverages regression techniques to estimate the coefficients of the polynomial expansion. More specifically, the QoI is evaluated at a number of sampling points, where the coefficients are computed by solving a linear system of equations, effectively fitting the polynomial chaos model to the observed data. Except from the typical regression-based PCE, the Adjoint-Assisted Regression-based PCE method has been proposed in [15]. This method requires not only the values of the QoI but also the sensitivity derivatives of the QoI with respect to the uncertain parameters. These sensitivity derivatives are computed using the adjoint method. The QoI values, along with the sensitivity derivatives, are then utilized to construct an overdetermined system of linear equations, which can be solved using methods, such as Least Squares or the Singular Value Decomposition (SVD) technique [7]. The adjoint-assisted regression-based PCE method reduces the cost of UQ by reducing the number of sampling points required to compute the coefficients of the PCE [15].

Overall, the ni-PCE with regression, especially when augmented with adjoint-assisted pieces of information, provides a robust and scalable framework for UQ in various complex systems.

1.1.2 Arbitrary PCE

Arbitrary PCE (aPCE), also known as Data-Driven PCE [14], is an advanced PCE variant that adapts the polynomial basis to the actual data distribution. Unlike traditional PCE, which relies on predefined orthogonal polynomials tailored to stan-

dard distributions (e.g., Gaussian, uniform), aPCE constructs a polynomial basis that best fits the empirical distribution of the input data.

The aPCE methodology involves the following steps: first, the probability distribution of the input data is analyzed to determine its key statistical properties, such as mean, variance, and higher-order moments. Next, an appropriate set of orthogonal polynomials is constructed to match this distribution. This adaptive approach allows the aPCE to handle non-standard and complex distributions that are often encountered in real-world applications.

One of the primary methods used in aPCE is the construction of orthogonal polynomials through the Mysovskikh process [13], applied to the input data set. This ensures that the resulting polynomials are orthogonal with respect to the empirical measure of the data. Regression techniques are then employed to determine the coefficients of the polynomial expansion, as in ni-PCE. By fitting the polynomial chaos model to the observed data, the aPCE can capture the underlying uncertainty more accurately.

The aPCE is particularly valuable in scenarios where the input data does not follow conventional probability distributions and by leveraging data-driven techniques, it enhances the flexibility and applicability of the PCE methods, providing more precise uncertainty quantification for complex and irregular data sets.

1.2 Thesis Objectives and Layout

The primary objective of this diploma thesis is to implement and enhance advanced methods for UQ within CFD frameworks using adjoint-assisted regression-based PCE, as well as arbitrary PCE. More specifically, it aims to develop and validate an efficient approach for quantifying uncertainty in engineering systems by combining non-intrusive PCE methods augmented with adjoint sensitivity information. The approach intends to significantly reduce computational expenses by decreasing the number of required simulations while maintaining high accuracy in predicting statistical moments of the QoI. To summarize, the implemented methods include regression-based generalized non-intrusive PCE, adjoint-assisted regression-based generalized non-intrusive PCE, regression-based arbitrary PCE, and quadrature-based arbitrary PCE.

To achieve these objectives, this thesis systematically addresses several key aspects:

Implementation and validation of generalized ni-PCE

The study will begin with implementing the generalized ni-PCE framework, examining its performance, and validating it through benchmark problems. Generalized ni-PCE refers to the ni-PCE method that can handle any type of conventional

probability distribution. This serves as a foundational step for understanding the complexities involved in UQ.

Integration of adjoint-assisted regression

Following the establishment of ni-PCE, this diploma thesis incorporates adjoint-assisted pieces of information to augment the regression process. The adjoint method provides sensitivity derivatives of the QoI, allowing for fewer model evaluations and subsequently reducing computational resources significantly compared to traditional regression methods.

Development of aPCE

This diploma thesis will also thoroughly develop the aPCE framework and explain its mathematical formulation, with the aim of tackling problems in which some or all uncertain variables do not follow conventional probability distributions.

Modeling of Shape Imperfections

The thesis incorporates the Karhunen-Loève Expansion (KLE) to effectively model and quantify the impact of geometric shape imperfections on aerodynamic performance. This approach accurately captures the variability arising from such imperfections, ensuring robust predictions in practical CFD applications.

Application to Engineering Cases

Finally, the methodologies developed in the thesis are applied and evaluated through several engineering test cases. These include assessing uncertainties in airfoil flow conditions, shape imperfections, and the performance metrics of a Supersonic Business Jet. Each case demonstrates the practical benefits and computational advantages of the adjoint-assisted regression-based PCE approach.

Chapter 2 presents the theoretical foundations and numerical implementations of ni-PCE and aPCE, emphasizing adjoint-assisted regression techniques. Chapter 3 introduces the mathematical formulation of the Karhunen-Loève Expansion and elaborates on its application to modeling shape imperfections. Chapter 4 provides detailed analyses and results from the implementation of the proposed UQ methods in selected engineering scenarios, focusing on computational efficiency and accuracy.

The four variations of PCE implemented in this thesis are compared in Table 1.1, highlighting their key characteristics.

PCE Method	**Basis Construction**	**Coefficient Computation**
Regression-Based Generalized PCE	Wiener-Askey polynomials	Least-Squares
Adjoint-Assisted Generalized PCE	Wiener-Askey polynomials	Least-Squares
Regression-Based aPCE	Data-driven orthogonal polynomials	Least-Squares
Quadrature-Based aPCE	Data-driven orthogonal polynomials	Numerical integration

Table 1.1: *Implemented PCE methodologies*

Chapter 2

Uncertainty Quantification

2.1 Non-Intrusive PCE

2.1.1 Formulation and Chaos Order

In the ni-PCE, the QoI which is dependent on the vector of uncertain variables $c_i, i \in [1, M]$, is approximated as

$$J(\vec{c}) \approx \sum_{i=0}^{Q-1} \alpha_i H_i(\vec{c}), \tag{2.1}$$

where M is the number of uncertain variables, Q is the total number of expansion terms, $H_i(\vec{c})$ the multi-dimensional orthogonal polynomials, and α_i the corresponding weights.

The upper bound of this expansion is referred as the chaos order (k) and corresponds to the highest degree of polynomial used in the series. This chaos order essentially controls the level of detail and the complexity of the model. A higher chaos order can capture more intricate interactions between the uncertain variables but at the cost of increased computational burden and the potential for overfitting if not managed correctly. Conversely, a lower chaos order simplifies the model, which may be beneficial for computational efficiency but might not adequately represent the underlying stochastic behavior, if the complexity of the true system is high. Selecting an appropriate chaos order is crucial for balancing accuracy and efficiency in stochastic modeling.

The multi-dimensional orthogonal polynomials $H_i(\vec{c})$ are constructed using a tensor

product expansion of the univariate orthogonal polynomials $h_i(c)$. The tensor product expansion involves taking the product of univariate polynomials $h_i(c)$ defined for each uncertain variable, thereby constructing multi-dimensional polynomials that preserve orthogonality across all input dimensions.

The total number of expansion terms Q can be determined using two different methods. In the first method, the expansion terms are limited by the one-dimensional polynomial order bounds p_j for the j-th uncertain parameter. This can be considered as the chaos order for a single uncertain variable within the entire set and is given by [3]:

$$Q = \prod_{j=1}^{M} (p_j + 1) \tag{2.2}$$

The second approach allows the chaos order k to be directly specified through the field of Combinatorics [23]. More specifically, the number of combinations of M integers with a sum lower than or equal to k is given by the following formula:

$$Q = \binom{M}{k} = \frac{(k+M)!}{k!M!} = \frac{(M+1)(M+2)\cdots(M+k)}{k!} \tag{2.3}$$

The distinction between the two methods lies in the way the chaos order is defined. In the second method, the user specifies the total chaos order k of the expansion, which represents a single value corresponding to the highest degree of the multivariate polynomial. Conversely, in the first method, the user specifies a set of values $\{p_j\}$, where each p_j denotes the highest degree of the univariate polynomial for each uncertain parameter, and the sum of these values equals the total chaos order k.

The first method has the advantage of allowing greater control over the maximum univariate polynomial order p_j for each uncertain parameter, enabling different maximum polynomial orders for individual variables. This characteristic is known as anisotropy. However, due to the frequent lack of such specific information, the second method is more commonly used. For the purposes of this work, the second method is utilized.

As shown in Table 2.1, the number of PCE coefficients (Q) to be computed increases exponentially with the chaos order and the number of uncertain variables. So, as this diploma thesis focuses on regression techniques for computing these coefficient computational cost increases dramatically with the complexity of the model. Later in this chapter, the adjoint-assisted regression technique that significantly reduces the computational cost of the PCE coefficients calculation.

The general form of each multi-dimensional orthogonal polynomial $H_i(\vec{c})$ is

Uncertain Variables (M)	PCE Coefficients Q
Chaos Order $k = 1$	
1	2
4	5
7	8
10	11
13	14
16	17
19	20
22	23
Chaos Order $k = 2$	
1	3
4	15
7	36
10	66
13	105
16	153
19	210
22	276
Chaos Order $k = 3$	
1	4
4	35
7	120
10	286
13	560
16	969
19	1540
22	2300

Table 2.1: *Number of PCE Coefficients for Different Numbers of Uncertain Variables and Chaos Orders.*

$$H_i(\vec{c}) = \prod_{l=1}^{M} h_{i_l}(c_l), \quad \sum_{l=1}^{M} i_l \leq k, \tag{2.4}$$

So, the index of the multi-dimensional orthogonal polynomial $H_i(\vec{c})$ scales with the chaos order k as

$$0 \leq i \leq Q - 1 \tag{2.5}$$

It should be noted that the input uncertain variables c_i must be standardized (mean value $\mu = 0$ and standard deviation $\sigma = 1$) and uncorrelated [6]. This ensures the orthogonality of the polynomials and homogeneity of the uncertain variables. In

case two or more variables are correlated with a known correlation coefficient, they should be decorrelated through an appropriate transformation to yield independent variables [6]. Methods that can spot the correlation between two or more variables include the Pearson correlation coefficient, the Spearman rank correlation coefficient, or the Kendall tau rank correlation coefficient [18].

The type of the 1D orthogonal polynomials used in equation 2.4 depends on the probability distribution of each uncertain parameter. The used polynomial type for the most common probability distributions is shown [24] in Table 2.2.

Distribution	**PDF**	**Polynomial**	**Support range**
Normal	$\frac{1}{\sqrt{2\pi}}e^{-\xi^2/2}$	Hermite	$(-\infty, \infty)$
Uniform	$\frac{1}{2}$	Legendre	$[-1, 1]$
Beta	$\frac{(1-\xi)^\alpha(1+\xi)^\beta}{2^{\alpha+\beta+1}B(\alpha+1,\beta+1)}$	Jacobi	$[-1, 1]$
Exponential	$e^{-\xi}$	Laguerre	$[0, \infty)$
Gamma	$\frac{\xi^\alpha e^{-\xi}}{\Gamma(\alpha+1)}$	Generalized Laguerre	$[0, \infty)$

Table 2.2: *Polynomial types for common probability distributions.*

For a better understanding of the construction of the multivariate orthogonal polynomials, a case with $M = 2$ uncertain variables and a general chaos order of $k = 2$ is assumed. The first variable is normally distributed and the second follows a beta distribution, so the Hermite and Jacobi polynomials are used, respectively. The total number of expansion terms is 6, as calculated by equation 2.3. The multidimensional orthogonal polynomials are constructed as follows:

$$H_0(c_1, c_2) = He_0(c_1)P_0(c_2), \tag{2.6}$$

$$H_1(c_1, c_2) = He_1(c_1)P_0(c_2), \tag{2.7}$$

$$H_2(c_1, c_2) = He_0(c_1)P_1(c_2), \tag{2.8}$$

$$H_3(c_1, c_2) = He_2(c_1)P_0(c_2), \tag{2.9}$$

$$H_4(c_1, c_2) = He_1(c_1)P_1(c_2), \tag{2.10}$$

$$H_5(c_1, c_2) = He_0(c_1)P_2(c_2). \tag{2.11}$$

2.1.2 Orthogonal Polynomials

This section details the expressions of the orthogonal polynomials listed in Table 2.2 and their corresponding derivatives, which are essential for the adjoint-assisted PCE.

Hermite Polynomials

We commence with the Hermite polynomials which are used to model the normal distribution. Hermite polynomials manifest in two distinct forms: the probabilistic H_{e_n} (which are used to model the normal distribution) and the physicist's H_n. Each variant is employed in different scientific domains, and their interrelation is explicated through the ensuing equation [1]:

$$H_{e_n}(x) = 2^{-n/2} H_n\left(\frac{x}{\sqrt{2}}\right) \tag{2.12}$$

The recursive definition for the probabilistic Hermite polynomial is as follows:

$$H_{e_{n+1}}(x) = xH_{e_n}(x) - nH_{e_{n-1}}(x), \quad H_{e_0}(x) = 1, \tag{2.13}$$

where $H_{e_0}(x) = 1$ and $H_{e_1}(x) = x$ constitute the initial terms of the probabilistic Hermite polynomials.

The norm of these polynomials within the weighted space w, which adheres to the standard normal distribution parameters $\mu = 0$ and $\sigma = 1$, is computed as follows [1]:

$$\|H_{e_k}\|_w^2 = \gamma_k = \langle H_{e_k}(x), H_{e_k}(x)\rangle_w = \int_{-\infty}^{\infty} H_{e_k}^2(x) w(x)\, dx = k! \tag{2.14}$$

and hence,

$$\|H_{e_k}\|_w = \sqrt{k!} \tag{2.15}$$

The standardized probabilistic Hermite polynomials are defined as follows:

$$\tilde{H}_{e_k}(x) := \frac{H_{e_k}(x)}{\|H_{e_k}\|_w} = \frac{H_{e_k}(x)}{\sqrt{k!}} \implies \|\tilde{H}_{e_k}(x)\|^2 = \gamma_k = 1, \quad \forall k = 0, 1, 2, \ldots \tag{2.16}$$

As per the derivative of the probabilistic Hermite polynomials, it can be proven that

$$\tilde{H}'_{k+1}(x) = \frac{d(\tilde{H}_{k+1})}{dx} = \sqrt{k+1} \cdot \tilde{H}_k(x) \tag{2.17}$$

Jacobi Polynomials

To model the beta distribution, the Jacobi polynomials are employed. These, denoted by $P_n^{(\alpha,\beta)}(x)$, are a class of orthogonal polynomials that are solutions to the Jacobi ODE:

$$(1-x^2)y'' + [\beta - \alpha - (\alpha+\beta+2)x]y' + n(n+\alpha+\beta+1)y = 0 \tag{2.18}$$

These polynomials are defined with a weight function $(1-x)^\alpha(1+x)^\beta$ on the interval $[-1,1]$, which matches the transformed form of the beta distribution's density function. This congruence allows the Jacobi polynomials to naturally accommodate the variety of shapes the beta distribution can assume, depending on the values α and β take on.

The recursive definition for the Jacobi polynomial $P_n^{(\alpha,\beta)}(x)$ is as follows:

$$P_{n+1}^{(\alpha,\beta)}(x) = (A_n x + B_n)P_n^{(\alpha,\beta)}(x) - C_n P_{n-1}^{(\alpha,\beta)}(x), \tag{2.19}$$

where:

$$A_n = \frac{(2n+\alpha+\beta+1)(2n+\alpha+\beta+2)}{2(n+1)(n+\alpha+\beta+1)}, \tag{2.20}$$

$$B_n = \frac{(\alpha^2-\beta^2)(2n+\alpha+\beta+1)}{2(n+1)(n+\alpha+\beta+1)(2n+\alpha+\beta)}, \tag{2.21}$$

$$C_n = \frac{(n+\alpha)(n+\beta)(2n+\alpha+\beta+2)}{(n+1)(n+\alpha+\beta+1)(2n+\alpha+\beta)} \tag{2.22}$$

The first two polynomials of the family are:

$$P_0^{(\alpha,\beta)}(x) = 1, \tag{2.23}$$

$$P_1^{(\alpha,\beta)}(x) = \frac{1}{2}(\alpha+\beta+2)x + \frac{1}{2}(\alpha-\beta) \tag{2.24}$$

In order to standardize the Jacobi polynomials (i.e, mean value $\mu = 0$ and standard deviation $\sigma = 1$), the following expression can be used to divide the polynomial obtained by the recursive definition.

$$\|P_n^{(\alpha,\beta)}\|^2 = \int_{-1}^{1} \left(P_n^{(\alpha,\beta)}(x)\right)^2 (1-x)^\alpha(1+x)^\beta \, dx \tag{2.25}$$

This integral can be computed analytically and the result is

$$\|P_n^{(\alpha,\beta)}\|^2 = \frac{2^{\alpha+\beta+1}}{2n+\alpha+\beta+1}\frac{\Gamma(n+\alpha+1)\Gamma(n+\beta+1)}{\Gamma(n+1)\Gamma(n+\alpha+\beta+1)} \tag{2.26}$$

and ,hence,

$$\|P_n^{(\alpha,\beta)}\| = \sqrt{\frac{2^{\alpha+\beta+1}}{2n+\alpha+\beta+1}\frac{\Gamma(n+\alpha+1)\Gamma(n+\beta+1)}{\Gamma(n+1)\Gamma(n+\alpha+\beta+1)}} \tag{2.27}$$

The k-th derivative of these polynomials is given by

$$\frac{d^k}{dz^k}P_n^{(\alpha,\beta)}(z) = \frac{\Gamma(\alpha+\beta+n+1+k)}{2^k\Gamma(\alpha+\beta+n+1)}P_{n-k}^{(\alpha+k,\beta+k)}(z), \tag{2.28}$$

where the Gamma Function $\Gamma(z)$ for a complex number z with $\mathrm{Re}(z) > 0$, is defined by the integral

$$\Gamma(z) = \int_0^\infty t^{z-1}e^{-t}\,dt. \tag{2.29}$$

This function extends the factorial to the complex plane, satisfying $\Gamma(n+1) = n!$ for all positive integers n.

It should be mentioned that the PDF of the beta distribution is not an exact match with the weight function of the Jacobi polynomials. So, a different normalization constant is needed to model accurately the beta distribution. Its PDF is given by

$$f(x;\alpha,\beta) = \frac{x^{\alpha-1}(1-x)^{\beta-1}}{B(\alpha,\beta)}, \quad \text{for } x \in [0,1], \tag{2.30}$$

where $B(\alpha,\beta)$ is the Beta function, defined as

$$B(\alpha,\beta) = \int_0^1 t^{\alpha-1}(1-t)^{\beta-1}\,dt. \tag{2.31}$$

Alternatively, it can be expressed in terms of the Gamma function:

$$B(\alpha,\beta) = \frac{\Gamma(\alpha)\Gamma(\beta)}{\Gamma(\alpha+\beta)}. \tag{2.32}$$

From the above equation and in order to match the weight function of the Jacobi

polynomials, it is clear that it should be chosen $\alpha = \beta - 1$, $\beta = \alpha - 1$ and carry out a change of variable $x = \frac{t+1}{2}$. Thus, $t = 2x - 1$.

So, from equation 2.25, we obtain

$$\int_0^1 P_n^{\alpha,\beta-1}(2x-1;\beta-1,\alpha-1)(1-(2x-1))^{\beta-1}(1+2x-1)^{\alpha-1}d(2x-1) =$$
$$-2^{\alpha+\beta-1}B(\alpha,\beta)\int_0^1 P_n^{\alpha,\beta-1}(2x-1;\beta-1,\alpha-1)\frac{x^{\alpha-1}(1-x)^{\beta-1}}{B(\alpha,\beta)}dx =$$
$$\frac{2^{\alpha+\beta-1}}{2n+\alpha+\beta-1}\frac{\Gamma(n+\alpha)\Gamma(n+\beta)}{\Gamma(n+\alpha+\beta-1)n!}\int_0^1 P_n^{\alpha,\beta-1}(2x-1;\beta-1,\alpha-1)f(x;\alpha,\beta)dx$$

Combining this equation with equation 2.26, we get

$$\int_0^1 P_n^2(2x-1;\beta-1,\alpha-1)\, f(x;\alpha,\beta)\,\mathrm{d}x = \frac{\Gamma(n+\alpha)\Gamma(n+\beta)}{(2n+\alpha+\beta-1)\Gamma(n+\alpha+\beta-1)n!B(\alpha,\beta)}$$

The equation above means that the L^2 norm of $P_n(2x-1;\beta-1,\alpha-1)$ with respect to the weight function $f(x;\alpha,\beta)$ is

$$\|P_n(2x-1;\beta-1,\alpha-1)\|_2 = \sqrt{\frac{\Gamma(n+\alpha)\Gamma(n+\beta)}{(2n+\alpha+\beta-1)\Gamma(n+\alpha+\beta-1)n!B(\alpha,\beta)}} \quad (2.33)$$

Legendre Polynomials

The Legendre polynomials are used to model the uniform distribution. The Legendre polynomials, denoted by $P_n(x)$, are a class of orthogonal polynomials that are solutions to the Legendre ODE:

$$\frac{d}{dx}\left[(1-x^2)\frac{dP_n}{dx}\right] + n(n+1)P_n = 0 \quad (2.34)$$

The Legendre polynomials are defined with a weight function $w(x) = 1$ on the interval $[-1, 1]$, which matches the transformed form of the uniform distribution's density function. They are a special case of the Jacobi polynomials with parameters

$\alpha = \beta = 0$ and their recursive definition is as follows:

$$P_{n+1}(x) = \frac{2n+1}{n+1} x P_n(x) - \frac{n}{n+1} P_{n-1}(x) \tag{2.35}$$

The first two polynomials of the family are:

$$P_0(x) = 1, \tag{2.36}$$

$$P_1(x) = x \tag{2.37}$$

The norm of these polynomials within the weighted space w, which adheres to the standard uniform distribution parameters $\mu = 0$ and $\sigma = 1$, is computed as follows:

$$\|P_n\|_w^2 = \gamma_n = \langle P_n(x), P_n(x) \rangle_w = \int_{-1}^{1} P_n^2(x) w(x)\, dx = \frac{2}{2n+1} \tag{2.38}$$

and hence,

$$\|P_n\|_w = \sqrt{\frac{2}{2n+1}} \tag{2.39}$$

Laguerre Polynomials

The exponential distribution is modeled using the Laguerre polynomials. The Laguerre polynomials, denoted by $L_n(x)$, are a class of orthogonal polynomials that are solutions to the Laguerre ODE:

$$x \frac{d^2 L_n}{dx^2} + (1 - x) \frac{dL_n}{dx} + n L_n = 0 \tag{2.40}$$

The Laguerre polynomials are defined with a weight function $w(x) = e^{-x}$ on the interval $[0, \infty)$, which matches the transformed form of the exponential distribution's density function. The recursive definition for the Laguerre polynomial $L_{n+1}(x)$ is as follows:

$$L_{n+1}(x) = \frac{2n+1-x}{n+1} L_n(x) - \frac{n}{n+1} L_{n-1}(x) \tag{2.41}$$

The first two polynomials of this family are:

$$L_0(x) = 1, \tag{2.42}$$

$$L_1(x) = 1 - x \tag{2.43}$$

The norm of these polynomials within the weighted space w, which adheres to the standard exponential distribution parameters $\mu = 0$ and $\sigma = 1$, is computed as follows:

$$\|L_n\|_w^2 = \gamma_n = \langle L_n(x), L_n(x) \rangle_w = \int_0^\infty L_n^2(x) w(x)\, dx = \frac{\Gamma(n+1)}{n!} \tag{2.44}$$

and, hence,

$$\|L_n\|_w = \sqrt{\frac{\Gamma(n+1)}{n!}} \tag{2.45}$$

The derivative of the Laguerre polynomials is given by the following recursive formula:

$$xL_n'(x) = nL_n(x) - nL_{n-1}(x) \tag{2.46}$$

Generalized Laguerre Polynomials

Finally, the Gamma distribution is modeled using the Generalized Laguerre polynomials. Denoted by $L_n^{(\alpha)}(x)$, these are a class of orthogonal polynomials that are solutions to the Generalized Laguerre differential equation:

$$xL_n''(x) + (\alpha + 1 - x)L_n'(x) + nL_n(x) = 0 \tag{2.47}$$

The Generalized Laguerre polynomials are defined with a weight function $w(x) = x^\alpha e^{-x}$ on the interval $[0, \infty)$, which matches the transformed form of the gamma distribution's density function. The recursive definition for the Generalized Laguerre polynomial $L_{n+1}^{(\alpha)}(x)$ is as follows:

$$L_{n+1}^{(\alpha)}(x) = \frac{(2n + 1 + \alpha - x)}{n+1} L_n^{(\alpha)}(x) - \frac{(n+\alpha)}{n+1} L_{n-1}^{(\alpha)}(x) \tag{2.48}$$

The first two polynomials of the family are:

$$L_0^{(\alpha)}(x) = 1, \tag{2.49}$$

$$L_1^{(\alpha)}(x) = 1 + \alpha - x \tag{2.50}$$

The norm of these polynomials within the weighted space w, which adheres to the standard gamma distribution parameters $\mu = 0$ and $\sigma = 1$, is computed as follows:

$$\|L_n^{(\alpha)}\|_w^2 = \gamma_n = \langle L_n^{(\alpha)}(x), L_n^{(\alpha)}(x) \rangle_w = \int_0^\infty L_n^{(\alpha)2}(x) w(x)\, dx = \frac{\Gamma(n+\alpha+1)}{n!} \tag{2.51}$$

and hence,

$$\|L_n^{(\alpha)}\|_w = \sqrt{\frac{\Gamma(n+\alpha+1)}{n!}} \tag{2.52}$$

The k-th derivative of the Generalized Laguerre polynomials is given by the following formula:

$$\frac{d^k}{dx^k} L_n^{(\alpha)}(x) = \begin{cases} (-1)^k L_{n-k}^{(\alpha+k)}(x) & \text{if } k \leq n \\ 0 & \text{otherwise} \end{cases} \tag{2.53}$$

Table 2.3 summarizes the expressions of the orthogonal polynomials for the most common probability distributions.

Polynomial	**Typical Expression**
Hermite	$H_{e_{n+1}}(x) = xH_{e_n}(x) - nH_{e_{n-1}}(x)$
Jacobi	$P_{n+1}^{(\alpha,\beta)}(x) = (A_n x + B_n)P_n^{(\alpha,\beta)}(x) - C_n P_{n-1}^{(\alpha,\beta)}(x)$
Legendre	$(n+1)P_{n+1}(x) = (2n+1)xP_n(x) - nP_{n-1}(x)$
Laguerre	$L_{n+1}(x) = \frac{2n+1-x}{n+1}L_n(x) - \frac{n}{n+1}L_{n-1}(x)$
Generalized Laguerre	$L_{n+1}^{(\alpha)}(x) = \frac{2n+1+\alpha-x}{n+1}L_n^{(\alpha)}(x) - \frac{n+\alpha}{n+1}L_{n-1}^{(\alpha)}(x)$

Table 2.3: *Typical expressions of various orthogonal polynomials.*

Polynomial	**Derivative Expression**
Hermite	$\tilde{H}'_{k+1}(x) = \frac{d(\tilde{H}_{k+1})}{dx} = \sqrt{k+1} \cdot \tilde{H}_k(x)$
Jacobi	$\frac{d^k}{dz^k}P_n^{(\alpha,\beta)}(z) = \frac{\Gamma(\alpha+\beta+n+1+k)}{2^k\Gamma(\alpha+\beta+n+1)}P_{n-k}^{(\alpha+k,\beta+k)}(z)$
Legendre	$\frac{d}{dx}P_{n+1}(x) = (n+1)P_n(x) + x\frac{d}{dx}P_n(x)$
Laguerre	$xL'_n(x) = nL_n(x) - nL_{n-1}(x)$
Generalized Laguerre	$\frac{d^k}{dx^k}L_n^{(\alpha)}(x) = (-1)^k L_{n-k}^{(\alpha+k)}(x), \quad \text{if } k \leq n$

Table 2.4: *Derivative expressions of various orthogonal polynomials.*

2.1.3 Galerkin Projection

The Galerkin projection method involves projecting the response onto each basis function (a set of orthogonal polynomials or other predefined functions used to construct the approximation). Projection decomposes the response into independent modes, isolating each uncertain parameter's contribution. This projection is

performed in order to compute the coefficients of the polynomial expansion that approximates the system's response. It utilizes the orthogonal properties of polynomials to determine each coefficient. From equation 2.1, the Galerkin projection method can be expressed as [3]

$$\alpha_i = \frac{\langle J(c), H_i(c) \rangle}{\langle H_i(c)^2 \rangle} = \frac{\int_\Omega J(c) H_i(c) \rho(\xi)\, d\xi}{\int_\Omega H_i(c)^2 \rho(\xi)\, d\xi}, \tag{2.54}$$

where $\rho(\xi) = \prod_{i=1}^{M} \rho_i(\xi_i)$ is the joint probability density function of the uncertain variables and $\Omega = \Omega_1 \otimes \cdots \otimes \Omega_M$ is the uncertain input parameter space.

The denominator in equation 2.54 is the norm squared of the multivariate orthogonal polynomial, which can be computed analytically and will be presented later in this chapter. The numerator is the inner product of the QoI and the multivariate orthogonal polynomial which cannot be computed analytically and requires the use of Gauss Quadrature. Gauss Quadrature with k points integrates exactly all polynomials of degree $2k-1$ or less. Since J and $H_i(c)$ are multiplied in equation 2.54, the highest order of the integrand is $2p_j$ in the j-th parameter dimension. This requires $p_j + 1$ quadrature points for exact integration in each dimension.

2.1.4 Regression

Instead of numerically integrating the inner product in equation 2.54, an alternative method can be used to approximate the coefficients α_i by means of regression [15]. In this approach, the QoI (J) is evaluated at L different c values and with equation 2.1, a linear system can be formed as

$$\begin{bmatrix} H_0(c_1) & \cdots & H_{Q-1}(c_1) \\ \vdots & \ddots & \vdots \\ H_0(c_L) & \cdots & H_{Q-1}(c_L) \end{bmatrix} \begin{bmatrix} \alpha_0 \\ \vdots \\ \alpha_{Q-1} \end{bmatrix} = \begin{bmatrix} J(c_1) \\ \vdots \\ J(c_L) \end{bmatrix} \tag{2.55}$$

with L equations and P unknowns. If $L = P$, then the system is determined and the coefficients α_i can be computed easily by inverting the matrix and multiplying it with the right-hand-side vector. To increase the accuracy of the regression, the number of samples L should be greater than the number of expansion terms P and, then, equation 2.55 corresponds to a least squares problem. Based on the literature, the number of samples should be at least three times the number of expansion terms (oversampling factor $r = 3$, $L = 3P$) [4].

The described overdetermined system with m equations and n unknowns can be solved with various methods, such as typical Least Squares or Singular Value Decomposition (SVD) method [21]. SVD is a powerful numerical method used to solve both overdetermined or underdetermined linear systems, perform matrix rank re-

duction, and compute pseudo-inverses. It provides a robust solution by decomposing the matrix into its singular values and corresponding singular vectors.

The SVD of a matrix $A \in \mathbb{R}^{m \times n}$ is given by:

$$A = U\Sigma V^T, \tag{2.56}$$

where U (with dimensions $m \times m$) and V (with dimensions $n \times n$) are the left and right singular vector matrices, respectively, and Σ (with dimensions $m \times n$) is a diagonal matrix containing the singular values of A. For the system $A\mathbf{x} = \mathbf{b}$, the solution that minimizes the least squares error $\|A\mathbf{x} - \mathbf{b}\|_2$ is given by:

$$\mathbf{x} = V\Sigma^+ U^T \mathbf{b}, \tag{2.57}$$

where Σ^+ (with dimensions $n \times m$) is the pseudo-inverse of Σ.

In practical terms, SVD provides a robust framework for solving linear systems, even when the matrix A is ill-conditioned or singular. By decomposing A into its singular values and vectors, SVD enables the stable computation of the coefficients α_i. This stability is especially valuable in uncertainty quantification, where the accurate determination of these coefficients is critical for reliable model predictions.

The only thing that remains is to decide the L different c values on which the QoI is to be evaluated. The most common approach is to use a Latin Hypercube Sampling (LHS) method. LHS is a stratified sampling technique that ensures a more uniform distribution of samples across the input parameter space. It divides the input space into intervals and selects one sample from each interval. This results in a more representative set of samples that captures the variability of the input parameters more effectively than random sampling.

2.1.5 Adjoint - assisted Regression

As it was previous mentioned, each row of the matrix of equation 2.55 corresponds to an evaluation of the QoI, which in certain cases can be computationally expensive. So, adding more lines in the matrix for each evaluation could accelerate the UQ process. This can be achieved by using the adjoint method to compute the sensitivity derivatives of the QoI with respect to the uncertain parameters. The computation of all the sensitivity derivatives $\frac{\delta J}{\delta c_i}, i \in [1, M]$ is of cost equivalent to that of a single QoI evaluation. The result is that with fewer sampling points (QoI evaluations), a satisfactory oversampling factor can be achieved and, thus, the UQ process can be

accelerated. The system of linear equations [15] that needs to be solved is now

$$\begin{bmatrix} H_0(c_1) & \cdots & H_{Q-1}(c_1) \\ \frac{\partial H_0}{\partial c_1}(c_1) & \cdots & \frac{\partial H_{Q-1}}{\partial c_1}(c_1) \\ \vdots & \ddots & \vdots \\ \frac{\partial H_0}{\partial c_M}(c_1) & \cdots & \frac{\partial H_{Q-1}}{\partial c_M}(c_1) \\ \vdots & \ddots & \vdots \\ H_0(c_L) & \cdots & H_{Q-1}(c_L) \\ \frac{\partial H_0}{\partial c_1}(c_L) & \cdots & \frac{\partial H_{Q-1}}{\partial c_1}(c_L) \\ \vdots & \ddots & \vdots \\ \frac{\partial H_0}{\partial c_M}(c_L) & \cdots & \frac{\partial H_{Q-1}}{\partial c_M}(c_L) \end{bmatrix} \begin{bmatrix} \alpha_0 \\ \vdots \\ \alpha_{Q-1} \end{bmatrix} = \begin{bmatrix} J(c_1) \\ \frac{\delta J}{\delta c_1}(c_1) \\ \vdots \\ \frac{\delta J}{\delta c_M}(c_1) \\ \vdots \\ J(c_L) \\ \frac{\delta J}{\delta c_1}(c_L) \\ \vdots \\ \frac{\delta J}{\delta c_M}(c_L) \end{bmatrix} \tag{2.58}$$

and can be solved with the SVD method as described in the previous section.

As mentioned in section 2.1.1, the input uncertain variables c_i should be standardized, meaning that they have zero mean and unit variance. In many cases though, the uncertain parameters ξ_i of the analysis are not standardized, thus the RHS of equation 2.58 should be adjusted accordingly (see below).

Apart from the sensitivity derivatives of the QoI, the derivatives of the multivariate orthogonal polynomials with respect to the uncertain parameters are also needed. These can be computed analytically, see table 2.4 .

The standardized uncertain variables c_i have the following properties:

$$\mu_{c_i} = 0, \quad \sigma_{c_i} = 1, \quad c_i^{\min} = -3, \quad c_i^{\max} = 3. \tag{2.59}$$

For the input unstandardized uncertain variables ξ_i:

$$\xi_i^{\min} = \mu_{\xi_i} - 3\sigma_{\xi_i}, \quad \xi_i^{\max} = \mu_{\xi_i} + 3\sigma_{\xi_i}. \tag{2.60}$$

To standardize ξ_i, we use:

$$\bar{\xi}_i = \frac{\xi_i - \xi_i^{\min}}{\xi_i^{\max} - \xi_i^{\min}} \in [0, 1]. \tag{2.61}$$

The relation between ξ_i and c_i is given by:

$$c_i = c_i^{\min} + \bar{\xi}_i \left(c_i^{\max} - c_i^{\min} \right) = c_i^{\min} + \frac{\xi_i - \xi_i^{\min}}{\sigma_{\xi_i}}, \tag{2.62}$$

which implies:

$$\xi_i = \xi_i^{\min} + \left(c_i - c_i^{\min}\right) \sigma_{\xi_i}. \tag{2.63}$$

Finally, the derivative of ξ_i with respect to c_i is:

$$\frac{\delta \xi_i}{\delta c_i} = \sigma_{\xi_i}. \tag{2.64}$$

So, by using the chain rule, each element of the RHS of equation 2.58 can be adjusted to:

$$\frac{\delta J}{\delta c_i} == \frac{\partial J}{\partial \xi_i} \frac{\partial \xi_i}{\partial c_i} = \frac{\partial J}{\partial \xi_i} \sigma_{\xi_i}. \tag{2.65}$$

The final form of the adjoint-assisted regression system is:

$$\begin{bmatrix} H_0(c_1) & \cdots & H_{Q-1}(c_1) \\ \frac{\partial H_0}{\partial c_1}(c_1) & \cdots & \frac{\partial H_{Q-1}}{\partial c_1}(c_1) \\ \vdots & \ddots & \vdots \\ \frac{\partial H_0}{\partial c_M}(c_1) & \cdots & \frac{\partial H_{Q-1}}{\partial c_M}(c_1) \\ \vdots & \ddots & \vdots \\ H_0(c_L) & \cdots & H_{Q-1}(c_L) \\ \frac{\partial H_0}{\partial c_1}(c_L) & \cdots & \frac{\partial H_{Q-1}}{\partial c_1}(c_L) \\ \vdots & \ddots & \vdots \\ \frac{\partial H_0}{\partial c_M}(c_L) & \cdots & \frac{\partial H_{Q-1}}{\partial c_M}(c_L) \end{bmatrix} \begin{bmatrix} \alpha_0 \\ \vdots \\ \alpha_{Q-1} \end{bmatrix} = \begin{bmatrix} J(c_1) \\ \frac{\partial J}{\partial \xi_1}(c_1)\sigma_{\xi_1} \\ \vdots \\ \frac{\partial J}{\partial \xi_M}(c_1)\sigma_{\xi_M} \\ \vdots \\ J(c_L) \\ \frac{\partial J}{\partial \xi_1}(c_L)\sigma_{\xi_1} \\ \vdots \\ \frac{\partial J}{\partial \xi_M}(c_L)\sigma_{\xi_M} \end{bmatrix} \tag{2.66}$$

2.1.6 Stochastic Moments Calculation

Having computed the coefficients α_i, the stochastic moments of the QoI can be calculated. The mean value and the variance of the QoI is given by [23]

$$\mu \approx \sum_{i=0}^{P-1} \alpha_i \langle H_i(c) \rangle = \alpha_0, \tag{2.67}$$

$$\sigma^2 \approx \sum_{i=0}^{P-1} \alpha_i^2 \langle H_i(c)^2 \rangle. \tag{2.68}$$

What remains is to compute the inner product of the multivariate orthogonal polynomials $\langle H_i(c)^2 \rangle$.

As described previously in this chapter, the multivariate orthogonal polynomials are constructed using a tensor product expansion of the univariate orthogonal polynomials. The Galerkin Projection of any two multivariate polynomials that belong to the same family and have orders i and j is given by

$$\begin{aligned}\langle H_i(\vec{x}), H_j(\vec{x})\rangle_W &= \int_{\mathbf{\Omega}} H_i(\vec{x})H_j(\vec{x})W(\vec{x})\,d\vec{x} \\ &= \int \cdots \int \left(\prod_{l=1}^{M} h_i(x_l)\right)\left(\prod_{l=1}^{M} h_j(x_l)\right)\left(\prod_{l=1}^{M} w_l(x_l)\right) dx_1 \cdots dx_M \\ &= \delta_{ij}\prod_{l=1}^{M}\int_{\Omega_l} h_i^2(x_l)w_l(x_l)\,dx_l = \delta_{ij}\int_{\mathbf{\Omega}} (H_i(\vec{x}))^2 W(\vec{x})\,d\vec{x}\end{aligned}$$

The above expression concludes to the simplified form

$$\langle H_i(\vec{x}), H_j(\vec{x})\rangle_W = \int_{\mathbf{\Omega}} H_i(\vec{x})H_j(\vec{x})W(\vec{x})\,d\vec{x} = \langle H_i(\vec{x}), H_i(\vec{x})\rangle_W \delta_{ij} \tag{2.69}$$

and by performing the same calculations as in equation 2.54, the final form of the inner product is

$$\begin{aligned}\langle H_i(\vec{x}), H_i(\vec{x})\rangle_W &= \int_{\mathbf{\Omega}} H_i^2(\vec{x})W(\vec{x})\,d\vec{x} \\ &= \prod_{l=1}^{M}\left(\int_{\Omega_l} h_i^2(x_l)w_l(x_l)\,dx_l\right) = \left(\prod_{l=1}^{M}\|h_i(x_l)\|_{w_l}\right)^2 \\ &= \|H_i(\vec{x})\|_W^2 = \gamma_n,\end{aligned}$$

which is simplified [23] to

$$\langle H_i(\vec{x}), H_i(\vec{x})\rangle_W = \|H_i(\vec{x})\|_W^2, \tag{2.70}$$

where $\|H_i(\vec{x})\|_W = \prod_{l=1}^{M}\|h_i(x_l)\|_{w_l}$ is the norm of the multivariate orthogonal polynomial.

The norms of the univariate orthogonal polynomials $\|h_i(x_l)\|_{w_l}$ are computed analytically and are given in table 2.5 for the most common probability distributions, see subsection 2.1.2.

Distribution	Norm of Polynomial	Polynomial
Normal	$n!$	Hermite (Probabilistic)
Uniform	$\frac{1}{2n+1}$	Legendre
Beta	$\frac{2^{\alpha+\beta+1}\Gamma(n+\alpha+1)\Gamma(n+\beta+1)}{(2n+\alpha+\beta+1)\Gamma(n+\alpha+\beta+1)\Gamma(n+1)}$	Jacobi
Exponential	$\frac{\Gamma(n+1)}{n!}$	Laguerre
Gamma	$\frac{\Gamma(n+\alpha+1)}{n!}$	Generalized Laguerre

Table 2.5: *Norms of polynomial types for common probability distributions.*

So, from equation 2.68, the variance of the QoI can be computed as

$$\sigma^2 = \sum_{i=0}^{\infty} \alpha_i^2 \int_{\Omega} H_i^2(\vec{x}) W(\vec{x})\, d\mathbf{x} = \sum_{i=0}^{\infty} \alpha_i^2 \|H_i(\vec{x})\|_W^2 = \sum_{i=0}^{\infty} \alpha_i^2 \gamma_i \tag{2.71}$$

2.1.7 A Mathematical Test Problem

In this section, the proposed methodology is applied to a benchmark problem, the Borehole function. The stochastic moments of the QoI are computed using the methodology outlined previously and the results are compared with the values obtained from Monte Carlo simulations, to validate the accuracy of the proposed methodology.

Borehole Function

The Borehole function [20] is a common benchmark problem used in the field of UQ. It is a mathematical model that describes the flow of water through a borehole $[m^3/year]$. The function is defined as follows:

$$F(\vec{x}) = \frac{2\pi T_u (H_u - H_l)}{\ln(r/r_w)\left[1 + \frac{2LT_u}{\ln(r/r_w)+(r_W)^2 K_w} + \frac{T_u}{T_l}\right]}, \tag{2.72}$$

The input variables $\vec{x} \in \mathbb{R}^8$ and their usual input ranges are given in table 2.6, while an illustration of the borehole is shown in figure 2.2.

Variable Range	Description
$r_w \in [0.05, 0.15]$	Radius of borehole (m)
$r \in [100, 50\,000]$	Radius of influence (m)
$T_u \in [63\,070, 115\,600]$	Transmissivity of upper aquifer (m^2/yr)
$H_u \in [990, 1110]$	Potentiometric head of upper aquifer (m)
$T_l \in [63.1, 116]$	Transmissivity of lower aquifer (m^2/yr)
$H_l \in [700, 820]$	Potentiometric head of lower aquifer (m)
$L \in [1120, 1680]$	Length of borehole (m)
$K_w \in [9855, 12\,045]$	Hydraulic conductivity of borehole (m/yr)

Table 2.6: *Input variables $\vec{x}$ and their ranges for the Borehole function.*

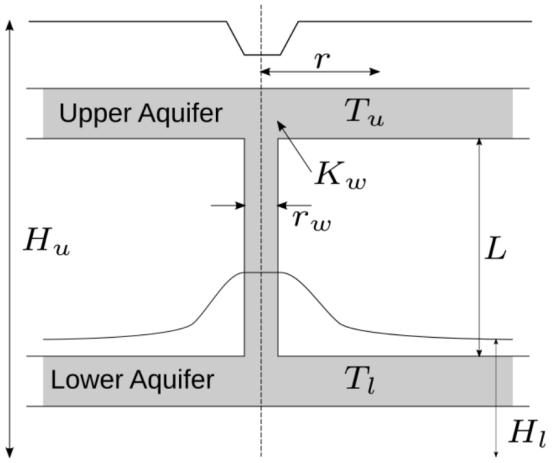

Figure 2.1: *Illustration for the water flow through the borehole*

For the purposes of UQ, the distributions of the input random variables are defined in Table 2.7.

Input Variable Distributions
$r_w \sim \mathrm{N}(\mu = 0.10, \sigma = 0.0161812)$
$r \sim \mathrm{Lognormal}(\mu = 7.71, \sigma = 1.0056)$
$T_u \sim \mathrm{Uniform}[63\,070, 115\,600]$
$H_u \sim \mathrm{Uniform}[990, 1110]$
$T_l \sim \mathrm{Uniform}[63.1, 116]$
$H_l \sim \mathrm{Uniform}[700, 820]$
$L \sim \mathrm{Uniform}[1120, 1680]$
$K_w \sim \mathrm{Uniform}[9855, 12\,045]$

Table 2.7: *Distributions of input variables for the Borehole function.*

Above, N(μ , σ^2) denotes a normal distribution with mean μ and standard deviation σ^2, while Uniform[a, b] denotes a uniform distribution with lower bound a and upper bound b. Longnormal(μ, σ^2) denotes a lognormal distribution with mean μ and standard deviation σ^2. In order to handle the Lognormal distribution, it is first transformed into a normal distribution by applying the natural logarithm to the random variable,

$$\xi = \ln(x)$$

A set of samples is generated using LHS from the input distributions. The QoI is then evaluated at each sample point using the Borehole function and the proposed methodology is applied to compute the stochastic moments of the QoI. ,Figure 2.2 illustrates the asymptotic convergence of the stochastic moments with increasing sample size, comparing the outcomes of Monte Carlo and the PCE.

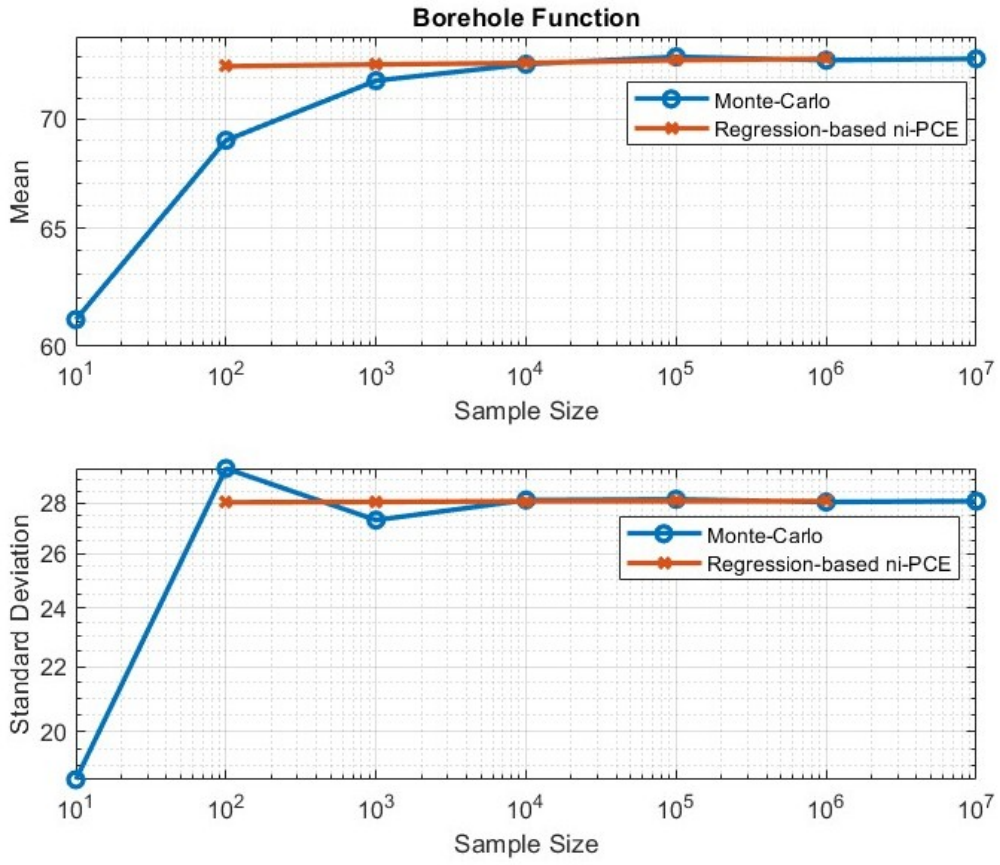

Figure 2.2: *Convergence of the Stochastic Moments for the Borehole Function using MC and the PCE with increasing sample size*

In the PCE approach, a chaos order of 2 was employed, resulting in a total of 45 terms in the expansion. The results indicate that the PCE method yields accurate estimates of the stochastic moments. Moreover, both the mean and standard deviation converge to their final values with a considerably smaller sample size than that

required by MC simulations. Specifically, with a sample size of 100 (an oversampling factor of 2.22), the PCE method accurately captures the stochastic moments, whereas the MC approach requires at least 100 times more samples to achieve comparable accuracy.

2.2 Arbitrary PCE

In many practical applications, input data do not adhere to standard probability distributions, making the conventional PCE method inapplicable. To overcome these limitations, the arbitrary PCE (aPCE) employs data-driven techniques to construct an orthogonal polynomial basis tailored to the observed data. This section provides an overview of the aPCE approach, discussing its theoretical foundations and its application in UQ.

2.2.1 Formulation of 1D aPCE

We consider a stochastic process defined on a probability space (Ω, A, Γ), where Ω represents the set of events, and Γ is the probability measure [9]. For a stochastic model $J = f(\xi)$, with the input $\xi \in \Omega$ and output J, the function $f(\xi)$ can be expanded using the PCE theory as:

$$J(\xi) \approx \sum_{i=0}^{Q} c_i P^{(i)}(\xi), \tag{2.73}$$

where in case of 1D PCE, $Q = k$, k being the order of expansion, c_i are the expansion coefficients that can be determined by the methods presented in the previous sections, and $P^{(i)}(\xi)$ are the polynomials forming the basis $\{P^{(0)}, \ldots, P^{(k)}\}$ that are orthogonal with respect to the measure Γ.

The distinction between aPCE and other PCE methods is that the measure Γ can have an arbitrary form, and thus the polynomial basis has to be found specifically for the probability measure Γ appearing in the respective application.

Once the polynomial basis is found and the expansion coefficients are determined using the aforementioned regression methods, the stochastic moments of the QoI can be computed using the expressions in subsection 2.1.6.

2.2.2 Formulation of multi-dimensional aPCE

If the model input $\vec{\xi}$, i.e. $\vec{\xi} = \{\xi_1, \xi_2, \ldots, \xi_N\}$ is multi-dimensional and the total number of stochastic parameters is equal to N , the expansion is formulated using

the multi-dimensional orthogonal polynomial basis:

$$J(\vec{\xi}) = J(\xi_1, \xi_2, \ldots, \xi_N) \approx \sum_{i=O}^{Q} c_i \Phi_i(\xi_1, \xi_2, \ldots, \xi_N), \tag{2.74}$$

where Φ_i is the multi-dimensional orthogonal polynomial basis and c_i are the expansion coefficients. The chaos order k of a multi-dimensional expansion was presented in detail in subsection 2.1.1. Finally, the stochastic moments of the QoI are computed in the same manner as in the 1D case, using the expressions in subsection 2.1.6.

To summarize, the distinctive and noteworthy aspect of the arbitrary Polynomial Chaos Expansion (aPCE) is not the formulation of the 1D and multi-dimensional expansions, but rather the construction of the orthogonal polynomial basis for the arbitrary probability measure Γ. In Section 2.2.3, the construction of the orthogonal polynomial basis for aPCE is presented in detail.

It should be noted that the current scientific understanding of polynomial chaos expansions requires that the random variables must either be statistically independent or exhibit only linear correlation. Linear correlations can be eliminated through appropriate linear transformations, such as the Karhunen-Loève (KL) expansion [10], also known as proper orthogonal decomposition [11] in some fields, or principal component analysis [16].

2.2.3 Construction of the Orthogonal Polynomial Basis for the aPCE

For the construction of the orthogonal polynomial basis for the aPCE the Mysovskikh theorem [13] is used. Firstly, let us define the polynomial $P^{(k)}(\xi)$ of degree k in the random variable $\xi \in \Omega$:

$$P^{(k)}(\xi) = \sum_{i=0}^{k} p_i^{(k)} \xi^i, \tag{2.75}$$

where $p_i^{(k)}$ are coefficients in $P^{(k)}(\xi)$.

The objective is to construct the polynomials in equation 2.75 to form an orthonormal basis for arbitrary distributions, using only the statistical moments obtained from the sample of the random variable ξ. With this methodology any given probability distribution defined solely by the statistical moments of ξ can be handled. This approach enables us to work with arbitrary probability measures that are implicitly and incompletely defined by a finite number of moments.

The orthonormality property for polynomials $P^{(k)}$ of degree k and $P^{(l)}$ of degree l is defined as:

$$\int_{\xi\in\Omega} P^{(k)}(\xi)P^{(l)}(\xi)d\Gamma(\xi) = \delta_{kl}, \quad \forall k,l = 0,\ldots,d \tag{2.76}$$

where δ_{kl} is the Kronecker delta.

For the continuation of the analysis, only the orthogonality condition will be utilized. Also, the leading coefficients of all polynomials will be set to 1. The orthonormality condition will be taken into account in the next step of the analysis. The orthogonality condition is given by:

$$\int_{\xi\in\Omega} P^{(k)}(\xi)P^{(l)}(\xi)d\Gamma(\xi) = 0, \quad \forall k \neq l. \tag{2.77}$$

With the help of equations 2.75 and 2.77, the generalized conditions of orthogonality for any polynomial $P^{(k)}$ of degree k with all lower-order polynomials can be written in the following form:

$$\int_{\xi\in\Omega} \left[p_0^{(0)} \sum_{i=0}^{k} p_i^{(k)}\xi^i\right] d\Gamma(\xi) = 0, \tag{2.78}$$

$$\int_{\xi\in\Omega} \left[\sum_{l=0}^{1} P_l^{(1)}\xi^l\right] \left[\sum_{i=0}^{k} P_i^{(k)}\xi^i\right] d\Gamma(\xi) = 0, \tag{2.79}$$

$$\vdots$$

$$\int_{\xi\in\Omega} \left[\sum_{l=0}^{k-1} P_l^{(k-1)}\xi^l\right] \left[\sum_{i=0}^{k} P_i^{(k)}\xi^i\right] d\Gamma(\xi) = 0, \tag{2.80}$$

$$p_k^{(k)} = 1. \tag{2.81}$$

The above system of equations is self-contained and determines the unknown polynomial coefficients $p_i^{(k)}$ (where $i = 0,\ldots,k$) for the desired basis. Notably, defining the orthogonal polynomial of degree k inherently relies on the definitions of all polynomials of preceding degrees $0,\ldots,k-1$. So, the system can by simplified by sequentially substituting each preceding equation into the subsequent one, starting

with the first equation into the second, then the first and second into the third, and continuing in this manner.

$$\int_{\xi\in\Omega}\left[\sum_{i=0}^{k} p_i^{(k)}\xi^i\right] d\Gamma(\xi) = 0, \tag{2.82}$$

$$\int_{\xi\in\Omega}\left[\sum_{i=0}^{k} p_i^{(k)}\xi^{i+1}\right] d\Gamma(\xi) = 0, \tag{2.83}$$

$$\vdots$$

$$\int_{\xi\in\Omega}\left[\sum_{i=0}^{k} p_i^{(k)}\xi^{k-1}\right] d\Gamma(\xi) = 0, \tag{2.84}$$

$$p_k^{(k)} = 1.$$

With this rearrangement, the k^{th} orthogonal polynomial is defined independent of all other polynomials from the orthogonal basis. As mentioned before, the analysis relies solely on the statistical moments of the random variable ξ. The k^{th} raw moment of the random variable ξ is defined as:

$$\mu_k = \int_{\xi\in\Omega} \xi^k d\Gamma(\xi) = \frac{1}{N}\sum_{i=1}^{N} \xi_i^k, \tag{2.85}$$

where N is the number of samples and ξ_i is the i^{th} sample of the random variable ξ. So, equations 2.82 to 2.84 can be rewritten based only on the raw moments of ξ:

$$\sum_{i=0}^{k} p_i^{(k)}\mu_i = 0 \tag{2.86}$$

$$\sum_{i=0}^{k} p_i^{(k)}\mu_{i+1} = 0 \tag{2.87}$$

$$\vdots$$

$$\sum_{i=0}^{k} p_i^{(k)}\mu_{i+k-1} = 0 \tag{2.88}$$

$$p_k^{(k)} = 1$$

or, in matrix form:

$$\begin{bmatrix} \mu_0 & \mu_1 & \cdots & \mu_k \\ \mu_1 & \mu_2 & \cdots & \mu_{k+1} \\ \vdots & \vdots & \ddots & \vdots \\ \mu_{k-1} & \mu_k & \cdots & \mu_{2k-1} \\ 0 & 0 & \cdots & 1 \end{bmatrix} \begin{bmatrix} p_0^{(k)} \\ p_1^{(k)} \\ \vdots \\ p_{k-1}^{(k)} \\ p_k^{(k)} \end{bmatrix} = \begin{bmatrix} 0 \\ 0 \\ \vdots \\ 0 \\ 1 \end{bmatrix}. \tag{2.89}$$

The next step is to normalize the aforementioned orthogonal polynomial basis in order to obtain an orthonormal basis and match the properties of the polynomials used in the previous sections. The normalization is performed using the norm of the polynomial $P^{(k)}$:

$$\left\| P^{(k)} \right\|^2 = \int_{\xi \in \Omega} \left[P^{(k)}(\xi) \right]^2 d\Gamma(\xi). \tag{2.90}$$

Thus, an orthonormal polynomial basis is:

$$\Psi^{(k)}(\xi) = \frac{1}{\|P^{(k)}\|} \sum_{i=0}^{k} p_i^{(k)} \xi^i. \tag{2.91}$$

Following a similar procedure as the one presented earlier, the matrix form of the orthonormal basis can be constructed:

$$\begin{bmatrix} \mu_0 & \mu_1 & \cdots & \mu_k \\ \mu_1 & \mu_2 & \cdots & \mu_{k+1} \\ \vdots & \vdots & \ddots & \vdots \\ \mu_k & \mu_{k+1} & \cdots & \mu_{2k} \end{bmatrix} \begin{bmatrix} p_0^{(\kappa)} \\ p_1^{(\kappa)} \\ \vdots \\ p_k^{(\kappa)} \end{bmatrix} = \begin{bmatrix} 0 \\ 0 \\ \vdots \\ \frac{1}{p_k^{(\kappa)}} \end{bmatrix} \tag{2.92}$$

where the left-hand side matrix is the Hankel Kernel matrix and is denoted with M [22].

As a consequence, an orthonormal polynomial basis up to order d can be constructed for any arbitrary probability measure Γ. if and only if the square matrix in the left-hand side of equation 2.92 is not singular.

The system of equations 2.92 can be solved using many different methods. One of the most fast and elegant ways is to perform Cholesky decomposition, i.e. by factoring a symmetric, Hermitian, positive-definite matrix into the product of a

lower triangular matrix and its conjugate transpose. In the context of the aPCE, the Cholesky decomposition is used, as the elements of the inverse of the upper triangular matrix are the coefficients of the orthonormal polynomial basis.

The Cholesky decomposition of the Hankel Kernel matrix in equation 2.92 is given by:

$$M = R^T R \quad \Rightarrow$$

$$\begin{bmatrix} \mu_0 & \mu_1 & \cdots & \mu_k \\ \mu_1 & \mu_2 & \cdots & \mu_{k+1} \\ \vdots & \vdots & \ddots & \vdots \\ \mu_k & \mu_{k+1} & \cdots & \mu_{2k} \end{bmatrix} = \begin{bmatrix} r_{11} & r_{12} & \cdots & r_{1,k+1} \\ 0 & r_{22} & \cdots & r_{2,k+1} \\ \vdots & \vdots & \ddots & \vdots \\ 0 & 0 & \cdots & r_{k+1,k+1} \end{bmatrix}^T \begin{bmatrix} r_{11} & r_{12} & \cdots & r_{1,k+1} \\ 0 & r_{22} & \cdots & r_{2,k+1} \\ \vdots & \vdots & \ddots & \vdots \\ 0 & 0 & \cdots & r_{k+1,k+1} \end{bmatrix}$$

Once the matrix R is obtained, a property from the Mysovskikh theorem [13] can be used to find the coefficients of the orthonormal polynomial basis from the inverse of the upper triangular matrix R.

The property states that:

$$R^{-1} = \begin{bmatrix} p_0^{(0)} & p_0^{(1)} & p_0^{(2)} & \cdots & p_0^{(k)} \\ \varnothing & p_1^{(1)} & p_1^{(2)} & \cdots & p_1^{(k)} \\ \varnothing & \varnothing & p_2^{(2)} & \cdots & p_2^{(k)} \\ \vdots & \vdots & \vdots & \ddots & \vdots \\ \varnothing & \varnothing & \varnothing & \cdots & p_k^{(k)} \end{bmatrix} \tag{2.93}$$

As a result, the coefficients of the orthonormal polynomial are computed and the orthonormal polynomial basis is constructed. In practice, the coefficient $p_i^{(k)}$ is obtained from the $(i+1, k+1)$ entry of R^{-1}, so that the k^{th} orthonormal polynomial can be expressed as

$$\Psi^{(k)}(\xi) = \frac{1}{\|P^{(k)}\|} \sum_{i=0}^{k} p_i^{(k)} \xi^i.$$

This expression offers a streamlined computational pathway, where the steps are: (i) assemble the Hankel Kernel matrix M from the moments of ξ, (ii) compute its Cholesky factorization $M = R^T R$, (iii) compute R^{-1}, and (iv) extract the polynomial coefficients directly from R^{-1} for constructing the orthonormal basis.

2.2.4 The aPCE using Regression

Once the orthonormal polynomials for the arbitrary probability measure Γ are constructed, the only step that remains is to compute the expansion coefficients. As mentioned in the previous sections, the expansion coefficients can be computed in a variety of ways, such as numerically integrating the inner product in equation 2.54 or using Regression methods. The same theory presented in subsection 2.1.4 can be applied to aPCE without any modifications. The only difference is on the left-hand-side matrix, where the polynomials are now the orthonormal polynomials constructed for the arbitrary probability measure Γ. It should be noted that in cases where some of the uncertain variables follow conventional probability distributions that were analyzed previously and others follow arbitrary probability distributions, the construction of the multivariate orthonormal polynomials is performed as presented in subsection 2.1.1 without any modifications. To put it differently, the multivariate polynomial of equation 2.4 is constructed from both the conventional and arbitrary polynomials.

In case regression is adjoint-assisted, as presented in subsection 2.1.5, and some or all of the uncertain variables follow arbitrary probability distributions, the derivatives of the multivariate orthogonal polynomials with respect to the uncertain parameters are needed. These can be computed analytically by differentiating the orthonormal polynomials constructed for the arbitrary probability measure Γ. The polynomials are given by equation 2.91:

$$\Psi^{(k)}(\xi) = \frac{1}{\|P^{(k)}\|} \sum_{i=0}^{k} p_i^{(k)} \xi^i.$$

The derivatives of the orthonormal polynomials with respect to the uncertain parameters are given by:

$$\frac{\partial \Psi^{(k)}(\xi)}{\partial \xi} = \frac{1}{\|P^{(k)}\|} \sum_{i=1}^{k} p_i^{(k)} i \xi^{i-1}. \tag{2.94}$$

So, the left-hand-side matrix of the adjoint system in equation 2.58 is constructed and the system can be solved using the SVD method as presented in subsection 2.1.5.

2.2.5 aPCE via Projection-Based Quadrature

In this approach, the expansion coefficients are computed by projecting the QoI onto the aPCE basis using an optimal quadrature rule. Specifically, if the orthonormal

basis $\{\Psi^{(i)}(\xi)\}_{i=0}^{k}$ has already been constructed for the arbitrary measure Γ (see Section 2.2.3), then the i^{th} coefficient is given by

$$c_i = \frac{\langle F, \Psi^{(i)} \rangle}{\langle \Psi^{(i)}, \Psi^{(i)} \rangle} \approx \frac{\sum_{j=1}^{N_q} w_j \, F(\xi_j) \, \Psi^{(i)}(\xi_j)}{\sum_{j=1}^{N_q} w_j \, \left[\Psi^{(i)}(\xi_j)\right]^2}, \tag{2.95}$$

where N_q is the number of quadrature nodes, $F(\xi)$ is the QoI, and $\{w_j, \xi_j\}$ are the quadrature weights and nodes, respectively. The basis is constructed to be orthonormal, hence $\langle \Psi^{(i)}, \Psi^{(i)} \rangle = 1$, so the coefficient simplifies to

$$c_i \approx \sum_{j=1}^{N_q} w_j \, F(\xi_j) \, \Psi^{(i)}(\xi_j). \tag{2.96}$$

A key aspect of the projection-based strategy is the generation of the quadrature rule. This is accomplished by leveraging the eigen-decomposition of the Jacobi matrix associated with the recurrence relation for the orthonormal polynomials. Although the construction of the orthonormal basis is presented in Section 2.2.3, here we explain how its optimal quadrature is obtained.

The three-term recurrence relation for the orthonormal polynomials can be written in compact form, and its coefficients are collected in the symmetric tridiagonal Jacobian matrix J:

$$J = \begin{bmatrix} a_0 & b_0 & & \\ b_0 & a_1 & \ddots & \\ & \ddots & \ddots & b_{k-1} \\ & & b_{k-1} & a_k \end{bmatrix}. \tag{2.97}$$

where a_i and b_i are the recurrence coefficients.

The eigenvalues of J are the optimal quadrature nodes (or collocation points) for integrating functions against Γ. The corresponding normalized eigenvectors provide the quadrature weights; specifically, if $v^{(j)}$ is the eigenvector corresponding to the node ξ_j, then the quadrature weight is computed as

$$w_j = \mu_0 \left[v_1^{(j)}\right]^2, \tag{2.98}$$

with μ_0 the zeroth moment of the measure (typically equal to one for a normalized probability measure) and $v_1^{(j)}$ the first component of $v^{(j)}$.

Once the univariate quadrature rules are available for each uncertain variable, the

multidimensional quadrature rule is obtained by forming a tensor product. For example, with $p+1$ nodes per variable and N independent variables, the overall quadrature rule contains $(p+1)^N$ nodes, with each multidimensional weight given by the product of the corresponding univariate weights. Thus, the full projection for the aPCE coefficient in the multidimensional setting becomes

$$c_k \approx \sum_{j=1}^{N_q} w_j \, F(\vec{\xi_j}) \, \Phi_k(\vec{\xi_j}), \tag{2.99}$$

where Φ_k is constructed as the tensor product of the univariate orthonormal polynomials.

2.2.6 Demonstration: Projection-Based Quadrature PCE

In this section, the projection-based quadrature procedure for an aPCE in a case in which the input variables are normally distributed is verified. A sampling size of 10^6 samples is used for each variable to safely estimate the required moments. Consider two random variables

$$\xi_1 \sim \mathcal{N}(2,1), \quad \xi_2 \sim \mathcal{N}(3,0.5),$$

and the QoI

$$F(\xi_1,\xi_2) = 4\,\xi_1 + 2\,\xi_2.$$

For this linear function the theoretical mean and standard deviation are

$$\mu_F = 4\times 2 + 2\times 3 = 14, \quad \sigma_F = \sqrt{4^2\times 1^2 + 2^2\times (0.5)^2} \approx 4.1231.$$

The objective of this verification is to confirm that the computed quadrature nodes, weights, and statistical moments match the classical Gauss–Hermite counterparts for normally distributed inputs. In our procedure, the aPCE method first constructs the univariate orthonormal polynomial bases from the input data. The quadrature nodes are then obtained as the eigenvalues of the corresponding Jacobi matrices, and the quadrature weights are determined as the square of the first component of the normalized eigenvectors. For normally distributed data, these nodes and weights should coincide with those from standard Gauss–Hermite quadrature after applying the affine transformation

$$x = \mu + \sigma\,\xi,$$

where ξ denotes a standard Gauss–Hermite node. The computations are performed for chaos order 3.

The values in Table 2.8 confirm that the quadrature-based evaluation recovers the mean and standard deviation of the QoI with high accuracy.

Quantity	Analytical Value	Computed Value
Mean	14.0000	13.997736
Std. Dev.	4.1231	4.120973

Table 2.8: *Statistical Moments of* $F(\xi_1, \xi_2) = 4\,\xi_1 + 2\,\xi_2$

Variable	Computed Nodes	Expected Gauss–Hermite Nodes
ξ_1	[-0.3323, 1.2600, 2.7421, 4.3351]	[-0.3344, 1.2580, 2.7420, 4.3344]
ξ_2	[1.8312, 2.6295, 3.3733, 4.1733]	[1.8328, 2.6290, 3.3710, 4.1672]

Table 2.9: *Collocation Points (Nodes) for Each Variable*

Variable	Computed Weights	Expected Weights
ξ_1	[0.0461, 0.4547, 0.4535, 0.0457]	[0.0459, 0.4541, 0.4541, 0.0459]
ξ_2	[0.0456, 0.4553, 0.4540, 0.0452]	[0.0459, 0.4541, 0.4541, 0.0459]

Table 2.10: *Quadrature Weights for Each Variable*

Table 2.9 shows that the computed collocation points for each variable align with the expected Gauss–Hermite nodes and Table 2.10 reports the quadrature weights computed for each variable.

Regarding the arbitrary polynomial basis, it is observed to closely approximate the Hermite polynomial basis, as expected. This outcome is justified by the fact that, although the aPCE methodology is employed, the underlying probability distributions of the uncertain variables are Gaussian. Figure 2.3 presents the first four orthonormal polynomials constructed via aPCE alongside the corresponding probabilist's Hermite polynomials for the first uncertain variable. The polynomial basis for the second uncertain variable exhibits similarly close agreement, as both variables follow a normal distribution.

2.2.7 Comparisson of quadrature-based and regression-based aPCE

In this section, the aaPCE methodology is applied to a mathematical function to demonstrate the accuracy of the regression-based aPCE, as well as the projection-based quadrature aPCE. For this purpose, the following function is considered:

$$J(X, Y) = 2X + 3Y, \tag{2.100}$$

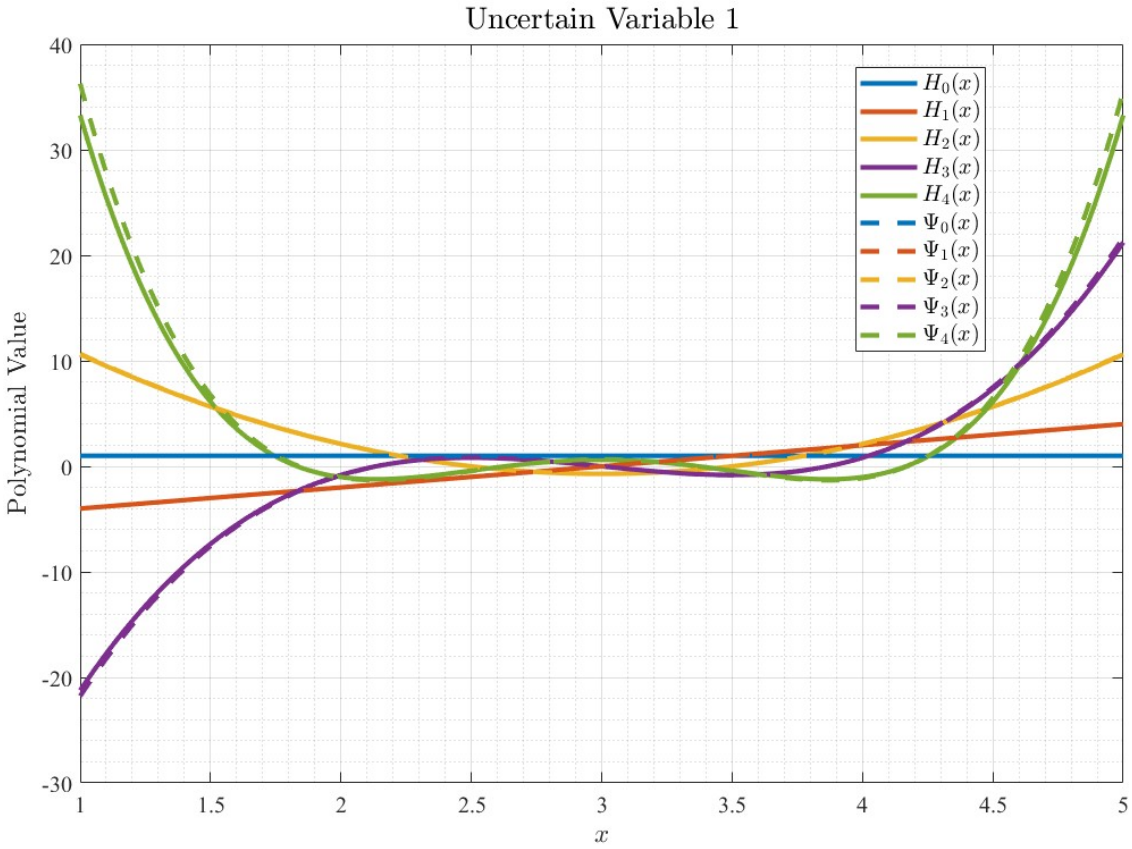

Figure 2.3: *Comparison of the aPCE and Hermite Polynomial Bases*

where $X \sim N(3, 0.2)$ and $Y \sim N(6, 0.4)$.

The above function has two uncertain parameters, X and Y, that follow normal distributions. The analytical mean value and variance of the QoI are given by:

$$\mu_J = 2\mu_X + 3\mu_Y = 2 \cdot 3 + 3 \cdot 6 = 24, \tag{2.101}$$

$$\sigma_J^2 = 2^2\sigma_X^2 + 3^2\sigma_Y^2 = 2^2 \cdot 0.2^2 + 3^2 \cdot 0.4^2 = 1.26491. \tag{2.102}$$

To validate the accuracy of the aPCE, a comparison is made between the ni-PCE with the distribution types of the input variables known and the aPCE with one or both of the distributions considered as arbitrary and the rest as known. In that case, the aPCE is used to construct the orthogonal polynomial basis for these distributions. The results are presented in table 2.11.

In conclusion, the results show that the aPCE method is able to accurately compute the stochastic moments of the QoI, even when the input variables are assumed to follow arbitrary probability distributions. As expected, the projection-based quadra-

Method	Distribution Type	Mean Value	STD
Analytical	$X \sim$ Gaussian, $Y \sim$ Gaussian	24	1.26491
ni-PCE – Regression	$X \sim$ Gaussian, $Y \sim$ Gaussian	24.0000	1.26491
aPCE – Regression	$X \sim$ Arbitrary, $Y \sim$ Gaussian	23.9766	1.25884
aPCE – Regression	$X \sim$ Gaussian, $Y \sim$ Arbitrary	24.0935	1.24375
aPCE – Regression	$X \sim$ Arbitrary, $Y \sim$ Arbitrary	24.0701	1.23758
aPCE – Quadrature	$X \sim$ Arbitrary, $Y \sim$ Arbitrary	23.997969	1.263522

Table 2.11: *Comparison of the Stochastic Moments for the QoI using ni-PCE and aPCE.*

ture aPCE method yields the best results among all the aPCE variations, with values that are nearly identical to the analytical ones. The aPCE is valuable when the distribution type is unknown or unconventional, making it an essential tool in UQ.

2.2.8 Application of the aPCE to Unknown Probability Distributions

This section demonstrates the application of the aPCE methodology to input uncertain variables governed by non-standard probability distributions. The aim is to evaluate the accuracy of aPCE-based quadrature in estimating the statistical moments of model compared to high-fidelity Monte Carlo simulations.

Problem Setup

Two uncertain input variables are constructed with distinctly non-Gaussian behavior. The first variable, denoted ξ_1, is a right-skewed Gaussian mixture, defined as a weighted combination of two normal distributions: 70% from $\mathcal{N}(3, 0.2^2)$ and 30% from $\mathcal{N}(3.5, 0.15^2)$. The second variable, ξ_2, follows a truncated normal distribution $\mathcal{N}(6, 0.4^2)$ restricted to the interval $[5.5, 6.5]$, and is further perturbed by a sinusoidal modulation to introduce oscillatory nonlinearity. The distributions are visualized in Figure 2.4, which presents both the empirical histograms and their corresponding Kernel Density Estimates (KDE) [19], overlaid with the quadrature nodes derived from aPCE.

The model under consideration is a simple linear combination of the input variables:

$$F(\xi_1, \xi_2) = 2\xi_1 + 3\xi_2, \tag{2.103}$$

which serves as the QoI for moment evaluation.

Methodology

The aPCE method is employed to construct the orthonormal polynomial basis for the two uncertain variables. The polynomial basis is then used to compute the expansion coefficients via a projection-based quadrature approach. The quadrature nodes and weights are derived from the eigenvalues and eigenvectors of the Jacobi matrix associated with the orthonormal polynomials. The statistical moments of the QoI are estimated using the aPCE expansion coefficients, and the results are compared against MC simulation with 10^8 samples, which serves as the benchmark for accuracy. The MC is performed by generating random samples from the defined distributions and evaluating the QoI at each sample point. The mean and standard deviation are then computed from the resulting sample set.

Numerical Results

The aPCE method yielded moment estimates in excellent agreement with the MC. For the MC simulation, a sample size of 10^8 was used, while the sample size for the aPCE quadrature was set to 10^4. Table 2.12 summarizes the computed mean and standard deviation using both approaches.

Method	**Mean**	**Standard Deviation**
Monte Carlo (Benchmark)	24.310578	1.006289
aPCE Quadrature	24.309736	1.006813

Table 2.12: *Comparison of statistical moments computed using MC and the aPCE-based quadrature*

The absolute errors were found to be $\mathcal{O}(10^{-4})$, confirming the capability of the aPCE to provide accurate estimates for arbitrarily shaped distributions.

Figure 2.4 illustrates the empirical PDFs for both input variables, while figure 2.5 presents the convergence behavior of the mean and standard deviation computed via Monte Carlo simulation as a function of increasing sample size. The horizontal lines represent the corresponding aPCE predictions, confirming convergence toward the quadrature-based values.

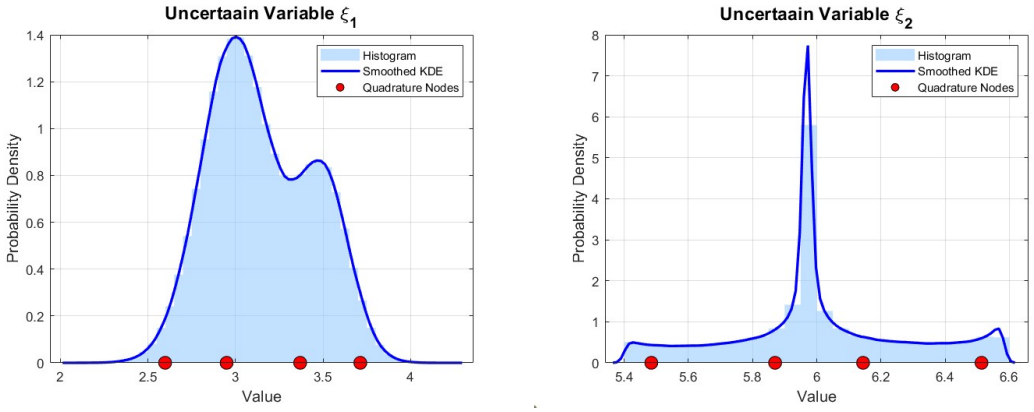

Figure 2.4: *Empirical PDFs of ξ_1 (left) and ξ_2 (right), shown with both histograms and kernel density estimates. Red markers indicate the locations of aPCE quadrature nodes.*

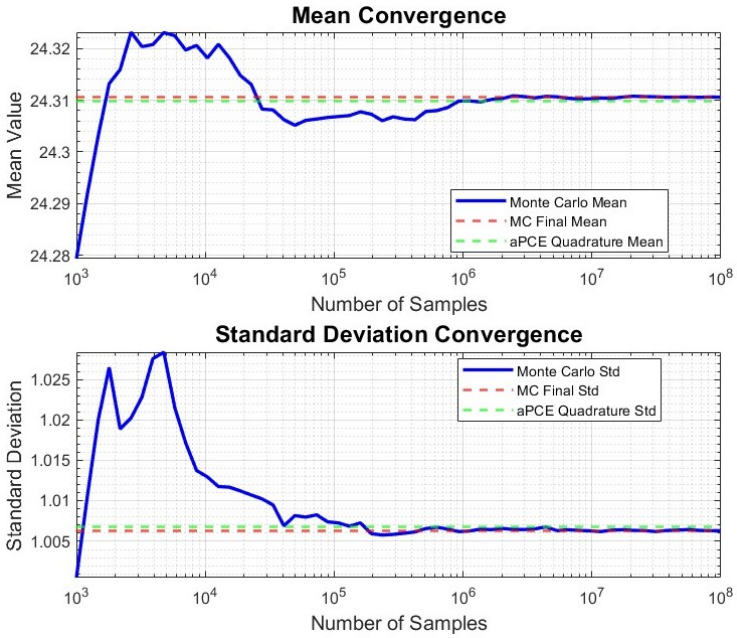

Figure 2.5: *Convergence of the Monte Carlo estimate of the mean (top) and standard deviation (bottom) as the number of samples increases. Horizontal dashed lines indicate the aPCE quadrature values.*

Chapter 3

Shape Imperfections

This chapter introduces the mathematical framework for stochastic processes used to model inevitable shape imperfections that arise during manufacturing. In the field of UQ, the term *shape imperfections* refers to the deviations of the manufactured part from the intended design. These deviations can be caused by a variety of factors, such as the manufacturing process, the material properties, and the tooling used. Although these deviations from the nominal geometry are often small, they can have a significant impact on the performance of the part. For example, in the case of a turbine blade, small deviations in the geometry can lead to changes in the aerodynamic performance of the blade, which can result in a decrease in efficiency. So, it is important to be able to quantify the impact of these shape imperfections on the performance of the part. A method that is widely used for this purpose is the Karhunen-Loève Expansion (KLE) [8], which is a mathematical framework for representing random fields. In this chapter, we will introduce the KLE and show how it can be used to model manufacturing imperfections.

3.1 Karhunen-Loève Expansion - Mathematical Formulation

The KLE is a mathematical framework for representing random fields. It is based on the idea that a random field can be decomposed into a sum of orthogonal modes, each of which has a certain variance. It offers a structured approach to representing random processes, addressing the challenge of dealing with abstract measure spaces that lack physical intuition. Unlike MC simulation, which requires a large number of random samples to approximate functions defined in these spaces, the KLE decomposes these functions into a series of orthogonal eigenfunctions. This approach

provides a systematic and efficient representation of the random field, capturing the essential characteristics of the process with fewer terms.

Based on the above, a random process $w(x, \theta)$ can be represented as:

$$w(x, \theta) = \sum_{n=0}^{\infty} \sqrt{\lambda_n} \xi_n(\theta) f_n(x) \tag{3.1}$$

where x denotes the position vector over the domain D, θ belongs to the space of random events Ω, $\{\xi_n(\theta)\}$ are random variables that need to be determined, λ_n are constants, and $\{f_n(x)\}$ are orthonormal deterministic functions. Also, $\bar{w}(x)$ represents the expected value across all realizations of the process.

The covariance function, $C(x_1, x_2)$, of the process is given by:

$$C(x_1, x_2) = \sum_{m=0}^{\infty} \lambda_m f_m(x_1) f_m(x_2) \tag{3.2}$$

where λ_m and $f_m(x)$ are eigenvalues and eigenfunctions of the covariance kernel, respectively. These are solutions to the integral equation:

$$\int_D C(x_1, x_2) f_n(x)\, dx_1 = \lambda_n f_n(x_2). \tag{3.3}$$

The eigenfunctions $f_n(x)$ form an orthonormal basis satisfy the normalization condition:

$$\int_D f_n(x) f_m(x)\, dx = \delta_{nm} \tag{3.4}$$

So, $w(x, \theta)$ in terms of its mean $\bar{w}(x)$ and a zero-mean random process $\alpha(x, \theta)$ can be expressed as following:

$$w(x, \theta) = \bar{w}(x) + \alpha(x, \theta) \tag{3.5}$$

where $\alpha(x, \theta)$ can be expanded in terms of the eigenfunctions as:

$$\alpha(x, \theta) = \sum_{n=0}^{\infty} \xi_n(\theta) \sqrt{\lambda_n} f_n(x). \tag{3.6}$$

The covariance function $C(x_1, x_2)$ can then be defined in terms of $\alpha(x, \theta)$ by taking

the expectation over θ:

$$C(x_1, x_2) = \mathbb{E}[\alpha(x_1, \theta)\alpha(x_2, \theta)]. \tag{3.7}$$

Expanding the expectation yields:

$$= \sum_{n=0}^{\infty} \sum_{m=0}^{\infty} \langle \xi_n(\theta)\xi_m(\theta) \rangle \sqrt{\lambda_n \lambda_m} f_n(x_1) f_m(x_2). \tag{3.8}$$

By orthogonality, each eigenfunction can be isolated through the equation:

$$\int_D C(x_1, x_2) f_k(x_2)\, dx_2 = \lambda_k f_k(x_1). \tag{3.9}$$

Further integration gives:

$$\lambda_k \int_D f_k(x_1) f_l(x_1)\, dx_1 = \sum_{n=0}^{\infty} \mathbb{E}[\xi_n(\theta)\xi_k(\theta)] \sqrt{\lambda_n \lambda_k} \delta_{nl} \tag{3.10}$$

where λ_k and δ_{kl} relate through the expectation $\langle \xi_k(\theta)\xi_l(\theta) \rangle$:

$$\lambda_k \delta_{kl} = \sqrt{\lambda_k \lambda_l} \langle \xi_k(\theta)\xi_l(\theta) \rangle. \tag{3.11}$$

This can be rearranged to confirm orthonormality of $\xi_n(\theta)$:

$$\langle \xi_k(\theta)\xi_l(\theta) \rangle = \delta_{kl}. \tag{3.12}$$

Thus, the random process $w(x, \theta)$ is represented as:

$$w(x, \theta) = \bar{w}(x) + \sum_{n=0}^{\infty} \xi_n(\theta) \sqrt{\lambda_n} f_n(x) \tag{3.13}$$

where the random variables $\xi_n(\theta)$ have zero mean and unit variance:

$$\langle \xi_n(\theta) \rangle = 0, \quad \langle \xi_n(\theta)\xi_m(\theta) \rangle = \delta_{nm} \tag{3.14}$$

By truncating the series in equation (3.13) past the Mth term, we obtain an approximation to $w(x, \theta)$ as follows:

$$w(x,\theta) = \bar{w}(x) + \sum_{n=0}^{M} \xi_n(\theta)\sqrt{\lambda_n} f_n(x). \tag{3.15}$$

The random variables $\xi_n(\theta)$ will later serve as the uncertain input variables in the test cases. So, what's left is to determine the eigenvalues λ_n and eigenfunctions $f_n(x)$, which can be obtained by solving the integral equation (3.3).

3.2 Eigenvalues and Eigenfunctions

As mentioned in the previous section, the eigenvalues λ_n and eigenfunctions $f_n(x)$ can be obtained by solving the integral equation (3.3). This equation can be rewritten as:

$$\int_D C(x_1, x_2) f(x_2)\, dx_2 = \lambda f(x_1). \tag{3.16}$$

Due to the properties of $C(x_1, x_2)$ (being bounded, symmetric, and positive definite), the eigenfunctions $f_i(x)$ and eigenvalues have specific properties:

- The set $f_i(x)$ is orthogonal and complete.

- Each eigenvalue λ_k has a finite number of linearly independent eigenfunctions.

- The eigenvalues form a countably infinite set.

- All eigenvalues are positive real numbers.

- The kernel $C(x_1, x_2)$ has the uniformly convergent expansion:

$$C(x_1, x_2) = \sum_{k=1}^{\infty} \lambda_k f_k(x_1) f_k(x_2). \tag{3.17}$$

The KLE thus leverages the properties of the covariance function, making it suitable for a variety of processes, including nonstationary and multidimensional ones. Suppose the process $\alpha(x, \theta)$ has a known rational spectrum of the form:

$$S(\omega) = \frac{N(\omega^2)}{D(\omega^2)} \tag{3.18}$$

where $N(\cdot)$ and $D(\cdot)$ are polynomials of order n and d, respectively. This structure implies the process has finite memory, suitable for processes with Markovian properties.

For stationary processes, equation (3.16) simplifies to:

$$\int_D C(x_1 - x_2) f(x_2)\, dx_2 = \lambda f(x_1) \tag{3.19}$$

which, for a 1D domain, can be expressed as:

$$f(x_2) \int_{-\infty}^{\infty} e^{i\omega|x_1 - x_2|} \frac{N(\omega^2)}{D(\omega^2)}\, d\omega = \lambda f(x_1). \tag{3.20}$$

Differentiating with respect to x_1 leads to:

$$\lambda D \left(\frac{d^2}{dx_1^2}\right) f(x_1) = \int_D N \left(\frac{d^2}{dx_2^2}\right) f(x_2) \delta(x_1 - x_2)\, dx_2 \tag{3.21}$$

where $\delta(\cdot)$ is the Dirac delta function.

The preceding treatment is applied to the exponential kernel, which for a 1D domain, is given by:

$$C(x_1, x_2) = \sigma^2 e^{-|x_1 - x_2|/l} \tag{3.22}$$

where l represents the correlation length, a parameter controlling the frequency of disturbances. At this point it is necessary to introduce the variable s, where $s \in [0, s_{\max}]$, with $s_{\max}$ representing the entire length of the contour of the shape being analyzed (in the case of this work, an airfoil). So, each point on the airfoil, with coordinates (x, y), corresponds to a specific value of s within the interval $[0, s_{\max}]$. From now on, s will be used instead of x to represent the position along the airfoil contour.

The parameter σ signifies the standard deviation of these disturbances and acts as a scaling factor for their magnitude. Although σ is not tied to a physical quantity, it standardizes the amplitude of the fluctuations. Therefore, for simplicity in this context, σ is set to 1 as the specific variation in imperfections is not quantified, making it effectively negligible.

So, with the use of the exponential kernel in equation (3.19), the integral solutions over a non-symmetric interval $D = [a, b]$, where $a, b \in \mathbb{R}$ and $s_1, s_2 \in D$, are expressed as:

$$\int_a^b \sigma^2 e^{-|s_1 - s_2|/l} f(s_2)\, ds_2 = \lambda f(s_1). \tag{3.23}$$

The correlation length l is often not precisely known, even to manufacturers. Thus,

in shape imperfection modeling, it is standard to assume $l = |a - b| = b - a$. For aerodynamic structures, where the interval D typically spans from $a = 0$ to $b = s_{\max}$, the correlation length is thus defined as $l = s_{\max}$, aligning with the earlier assumption.

Equation (3.23) can be rewritten as:

$$\int_a^s e^{-c|s_1-s_2|} f(s_2)\, ds_2 + \int_s^b e^{-c|s_1-s_2|} f(s_2)\, ds_2 = \lambda f(s_1) \tag{3.24}$$

where $c = \frac{1}{l} = \frac{1}{b-a}$.

Differentiating the above equation with respect to s_1 gives:

$$\lambda f'(s_1) = -c \int_a^s e^{-c(s_1-s_2)} f(s_2)\, ds_2 + c \int_s^b e^{c(s_1-s_2)} f(s_2)\, ds_2. \tag{3.25}$$

By differentiating one more time w.r.t s_1, the following is obtained:

$$\lambda f''(s) = \left(-2c + c^2\lambda\right) f(s). \tag{3.26}$$

Finally, by introducing the following new variable:

$$\omega^2 = \frac{2c - c^2\lambda}{\lambda} \tag{3.27}$$

the differential equation becomes:

$$f''(s) + \omega^2 f(s) = 0, \quad a \le s \le b \tag{3.28}$$

So, the integral equation (3.23) is transformed into an Ordinary Differential Equation (ODE) with the following boundary conditions:

$$cf(a) - f'(a) = 0, \tag{3.29}$$

$$cf(b) + f'(b) = 0. \tag{3.30}$$

It can be shown that $\omega^2 \ge 0$ is the only range of ω for which (3.28) is solvable. The solution is given by:

$$f(s) = \alpha_1 \cos\left[\omega\left(s - \frac{a+b}{2}\right)\right] + \alpha_2 \sin\left[\omega\left(s - \frac{a+b}{2}\right)\right] \tag{3.31}$$

where α_1 and α_2 are constants to be determined.

By substituting (3.31) into the boundary conditions (3.29) and (3.30), the following system of equations is obtained:

$$\begin{cases} \alpha_1\left[1 - \omega l \tan\left(\omega\frac{b-a}{2}\right)\right] - \alpha_2\left[\tan\left(\omega\frac{b-a}{2}\right) + \omega l\right] = 0, \\ \alpha_1\left[1 - \omega l \tan\left(\omega\frac{b-a}{2}\right)\right] + \alpha_2\left[\tan\left(\omega\frac{b-a}{2}\right) + \omega l\right] = 0. \end{cases} \tag{3.32}$$

Non-trivial solutions exist only when the determinant J of the homogeneous system equals to zero:

$$J = 2\left[\omega l + \tan\left(\omega\frac{b-a}{2}\right)\right]\left[1 - \omega l \tan\left(\omega\frac{b-a}{2}\right)\right] = 0. \tag{3.33}$$

This leads to the following transcendental equations:

$$\underline{\text{For odd values of } \omega}: \quad c - \omega \tan\left(\omega\frac{b-a}{2}\right) = 0. \tag{3.34}$$

$$\underline{\text{For even values of } \omega}: \quad \omega + c \tan\left(\omega\frac{b-a}{2}\right) = 0. \tag{3.35}$$

In conclusion, the eigenfunctions are given by:

$$f(s) = \begin{cases} \frac{\cos\left(\omega\left(s-\frac{a+b}{2}\right)\right)}{\sqrt{\frac{b-a}{2} + \frac{\sin(\omega(b-a))}{2\omega}}}, & \text{for } n \text{ even} \\ \frac{\sin\left(\omega\left(s-\frac{a+b}{2}\right)\right)}{\sqrt{\frac{b-a}{2} - \frac{\sin(\omega(b-a))}{2\omega}}}, & \text{for } n \text{ odd} \end{cases} \tag{3.36}$$

The corresponding eigenvalues can be obtained through equation (3.27):

$$\lambda_n = \frac{2l}{1 + (\omega l)^2}. \tag{3.37}$$

3.3 Derivative of the KLE w.r.t the Uncertain Variables

As discussed in section 2.1.5, in order to form the system of linear equations 2.58 for the regression-based PCE, the derivative of the QoI with respect to the random variables c_n is required. In case the uncertainty arises from manufacturing imperfections and is modeled using the KLE, it is necessary to calculate the derivative of the expansion with respect to the uncertain variables ξ_n.

Using the chain rule, the derivative of the QoI with respect to the random variables can be expressed as:

$$\frac{\partial J}{\partial c_n} = \frac{\partial J}{\partial \mathbf{x}} \frac{\partial \mathbf{x}}{\partial c_n}. \tag{3.38}$$

In the cases that this work focuses on, the first term in equation (3.38) is calculated directly using the adjoint method in CFD. The second term, which in the case of shape imperfections, is the derivative of the KLE with respect to the random variables and is calculated as follows:

$$\frac{\partial X_{KLE}(s,c)}{\partial c_n} = \frac{\partial}{\partial c_n}\left(\bar{X_{KLE}}(s) + \sum_{n=0}^{M} c_n \sqrt{\lambda_n} f_n(x)\right) = \sqrt{\lambda_n} f_n(s). \tag{3.39}$$

It's important to note that equation (3.39) is expressed in terms of the variable s, which represents the position along the airfoil contour. However, for practical applications, it's necessary to transform this expression into the Cartesian coordinates (x, y). This transformation incorporates scaling factors determined by the geometry and manufacturing imperfections.

The transformation involves four key scaling parameters:

Hanning Window Coefficient $C_{\mathbf{Hann}}(s)$

The Hanning window is applied to taper the perturbations near the boundaries of a geometry to ensure a smooth geometry transition. This is achieved using a weighted cosine function. The coefficient $C_{\text{Hann}}(s)$ is defined as:

$$C_{\text{Hann}}(s) = \begin{cases} 1 - \cos\left(\frac{\pi}{2ps_{\max}} s\right), & \text{for } s < ps_{\max} \\ 1, & \text{for } ps_{\max} \leq s \leq (1-p)s_{\max}, \\ 1 - \cos\left(\frac{\pi}{2ps_{\max}}(1-s)\right), & \text{for } s > (1-p)s_{\max} \end{cases} \tag{3.40}$$

where p is the user-defined percentage of the contour length $s_{\max}$ where the damping should occur. For instance, if $p = 0.08$, damping is applied to 8% of the airfoil contour near the leading and trailing edges.

After incorporating this coefficient, the updated Karhunen-Loève expansion becomes:

$$X_{KLE}(s, c) = \bar{X}(s) + C_{\text{Hann}}(s) \sum_{n=1}^{M} \sqrt{\lambda_n} c_n f_n(s). \tag{3.41}$$

The derivative of the Hanning-windowed KLE expansion with respect to c_n is:

$$\frac{\partial X_{KLE}(s, c)}{\partial c_n} = C_{\text{Hann}}(s) \sqrt{\lambda_n} f_n(s), \tag{3.42}$$

assuming $C_{\text{Hann}}(s)$ is independent of c_n.

Maximum Scaling a_{maxh}

This is derived from the maximum deviation of the geometry, normalized to ensure the contours match the maximum user-defined imperfection height d_{height}. Mathematically:

$$a_{\text{maxh}} = \max_s |X_{KLE}(s, c)|. \tag{3.43}$$

The derivative of a_{maxh} with respect to the random variables c_n is non-trivial due to the dependence of $X_{KLE}(s, c)$ on c_n.

Imperfection Height Scaling d_{height}

This is a user-defined maximum imperfection height and acts as a fixed multiplier:

$$X_{KLE,\text{scaled}}(s, c) = \frac{X(s, c)}{a_{\text{maxh}}} d_{\text{height}}. \tag{3.44}$$

The derivative of the transformed geometry with respect to c_n, considering the chain

rule, can be expressed as:

$$\frac{\partial X(s,c)}{\partial c_n} = \frac{\partial X_{KLE}(s,c)}{\partial c_n} \cdot \frac{d_{\text{height}}}{a_{\text{maxh}}} + X_{KLE}(s,c) \cdot \frac{\partial}{\partial c_n}\left(\frac{d_{\text{height}}}{a_{\text{maxh}}}\right), \tag{3.45}$$

where $\frac{\partial X_{KLE}(s,c)}{\partial c_n}$ is calculated from equation (3.39).

To compute the derivative of a_{maxh} with respect to c_n, the position $s_{\max}$ where $a_{\text{maxh}} = |X(s_{\max}, c)|$ must be determined. Assuming $a_{\text{maxh}} = |X(s_{\max}, c)|$, the derivative becomes:

$$\frac{\partial a_{\text{maxh}}}{\partial c_n} = \text{sign}(X_{KLE}(s_{\max}, c)) \cdot \frac{\partial X_{KLE}(s_{\max}, c)}{\partial c_n}. \tag{3.46}$$

Normal Direction Transformation

The transformation also involves the unit normal to the airfoil contour directions N_x and N_y, defined as:

$$N_x = \frac{\partial y(s)}{\partial s}, \quad N_y = -\frac{\partial x(s)}{\partial s}, \tag{3.47}$$

normalized by their magnitude:

$$\text{norm} = \sqrt{N_x^2 + N_y^2}, \quad N_x \leftarrow \frac{N_x}{\text{norm}}, \quad N_y \leftarrow \frac{N_y}{\text{norm}}. \tag{3.48}$$

The perturbed geometry in Cartesian coordinates is then given by:

$$x_{KLE,out} = x_{initial} + N_x \cdot X_{KLE,scaled}, \quad y_{KLE,out} = y_{initial} + N_y \cdot X_{KLE,scaled}. \tag{3.49}$$

Final Expression Using Chain Rule

Combining all the transformations and scaling factors, the derivative of the perturbed geometry in Cartesian coordinates with respect to the uncertain variables c_n can be expressed as:

$$\frac{\partial x_{KLE,out}(s,c)}{\partial c_n} = \frac{\partial y(s)}{\partial s} \cdot \Bigg(C_{\text{Hann}}(s)\sqrt{\lambda_n} f_n(s) \cdot \frac{d_{\text{height}}}{a_{\text{maxh}}} - X_{KLE}(s,c) \cdot \frac{d_{\text{height}}}{a_{\text{maxh}}^2} \cdot \text{sign}(X_{KLE}(s_{\max},c)) \cdot C_{\text{Hann}}(s_{\max})\sqrt{\lambda_n} f_n(s_{\max}) \Bigg), \tag{3.50}$$

$$\frac{\partial y_{KLE,out}(s,c)}{\partial c_n} = -\frac{\partial x(s)}{\partial s} \cdot \Bigg(C_{\text{Hann}}(s)\sqrt{\lambda_n} f_n(s) \cdot \frac{d_{\text{height}}}{a_{\text{maxh}}} - X_{KLE}(s,c) \cdot \frac{d_{\text{height}}}{a_{\text{maxh}}^2} \cdot \text{sign}(X_{KLE}(s_{\max},c)) \cdot C_{\text{Hann}}(s_{\max})\sqrt{\lambda_n} f_n(s_{\max}) \Bigg). \tag{3.51}$$

Here:

- $C_{\text{Hann}}(s)$ is the damping coefficient, ensuring smooth transitions at the boundaries,
- $\sqrt{\lambda_n} f_n(s)$ is the contribution of the n-th eigenmode to the geometry perturbation,
- $\frac{d_{\text{height}}}{a_{\text{maxh}}}$ scales the perturbation to the desired imperfection height.

These final expressions capture the full dependency of the perturbed airfoil geometry on the uncertain variables c_n, incorporating all transformations, damping effects, and scaling factors.

Chapter 4

Test Cases in UQ

This chapter presents a systematic evaluation of adjoint-assisted regression-based PCE and aPCE methods through three test cases of various complexity. The studies validate the computational framework while assessing performance across different regimes of stochastic dimensionality in aerospace applications.

Section 4.1 examines a NACA 4415 airfoil with two uncertain flow parameters, establishing comparisons between traditional and adjoint-enhanced PCE methods. Results demonstrate sub-0.1% accuracy in moment estimation with computational savings exceeding 90% compared to conventional regression PCE.

Section 4.2 investigates an n16103 airfoil with 18 geometric uncertainties modeled through KLE. The adjoint approach provides critical efficiency advantages, achieving tenfold cost reductions compared to conventional regression PCE.

Section 4.3 evaluates a complete Supersonic Business Jet configuration with 12 coupled design variables. The analysis demonstrates sub-1% errors in performance metrics versus MC while significantly reducing computational costs.

These case studies form a comprehensive validation hierarchy from fundamental benchmarks to industrial applications.The consistent methodology enables clear assessment of the adjoint approach's scalability and robustness.

4.1 Case 1: Airfoil with Uncertain Flow Conditions

The first test case is related to the NACA 4415 airfoil. The objective is to quantify uncertainties in the Lift and Drag resulting from variations in the free-stream ve-

locity and angle of attack (AoA). CFD simulations are conducted using the PUMA software developed by the Parallel CFD & Optimization Unit of the NTUA[2], which solves the Euler equations using a finite volume method. Because the flow is assumed inviscid (thus governed by the Euler equations), the presence of a shock wave is required for drag to be developed. The NACA 4415 airfoil geometry is illustrated in Figure 4.1.

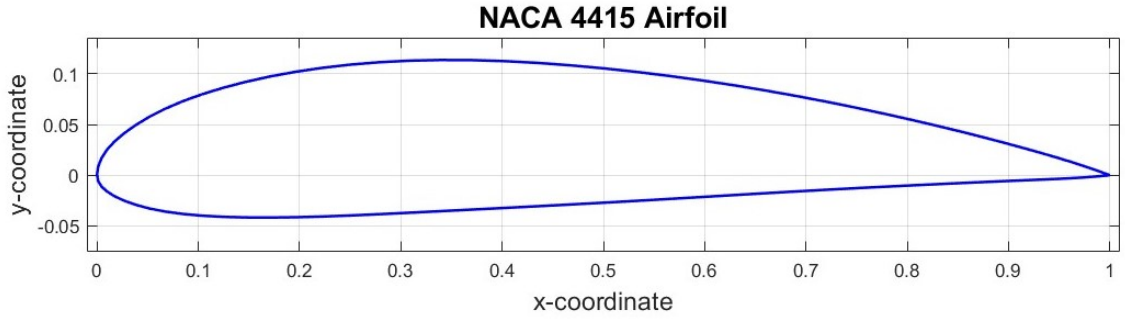

Figure 4.1: *The naca4415 airfoil.*

For this case, the aforementioned uncertainties are modeled as follows. The free-stream velocity is assumed to follow a Normal distribution with a mean value of 240 m/s and a standard deviation of 0.33 m/s, i.e., $\mathcal{N}(240, 0.33^2)$. The AoA is modeled using a Beta distribution with shape parameters $\alpha = 1$ and $\beta = 2$, bounded between 1.6 and 2.5 degrees.

While the small number of uncertain variables suggests that a GQ-based PCE is the most suitable approach, this case serves as an introductory example to demonstrate the application of the adjoint-assisted, regression-based PCE in CFD. A comprehensive comparison between the two methods will be provided in Section 4.2, where the latter approach will be the only feasible option.

Benchmark Analysis: GQ-based PCE

To establish a reference solution for UQ in the Lift and Drag due to input variability, a GQ - based PCE approach is adopted. This method is especially effective in low-dimensional stochastic problems, offering high accuracy at relatively low computational cost.

The quadrature rules are selected according to the type of input distributions. Specifically, Gauss–Hermite quadrature is used for the free-stream velocity, while Gauss–Jacobi quadrature is adopted for the AoA, with appropriate scaling to match the physical bounds. A tensor-product of univariate rules is used to construct the multivariate quadrature scheme over the joint probability space. The QoIs are evaluated at each node, and the associated statistical moments are computed using the corresponding quadrature weights. This benchmark is performed using a chaos order

of 2, resulting in a total of 9 quadrature nodes, thus 9 CFD runs for the computation of the sought statistical moments.

The results of this benchmark analysis are summarized in Table 4.1, providing a reference for assessing the accuracy of adjoint-assisted regression-based PCE models introduced later. These values represent the expected behavior of the Lift and Drag under the specified uncertainties in flow conditions.

QoI	Mean	Standard Deviation
Lift [N]	336.54131	8.40852
Drag [N]	20.21745	1.42208

Table 4.1: *Benchmark statistics for Lift and Drag using GQ-based PCE.*

Figure 4.2 displays the pressure distribution around the NACA 4415 airfoil at one of the GQ nodes. This visualization highlights the shock wave formation induced by the airfoil's aerodynamic performance.

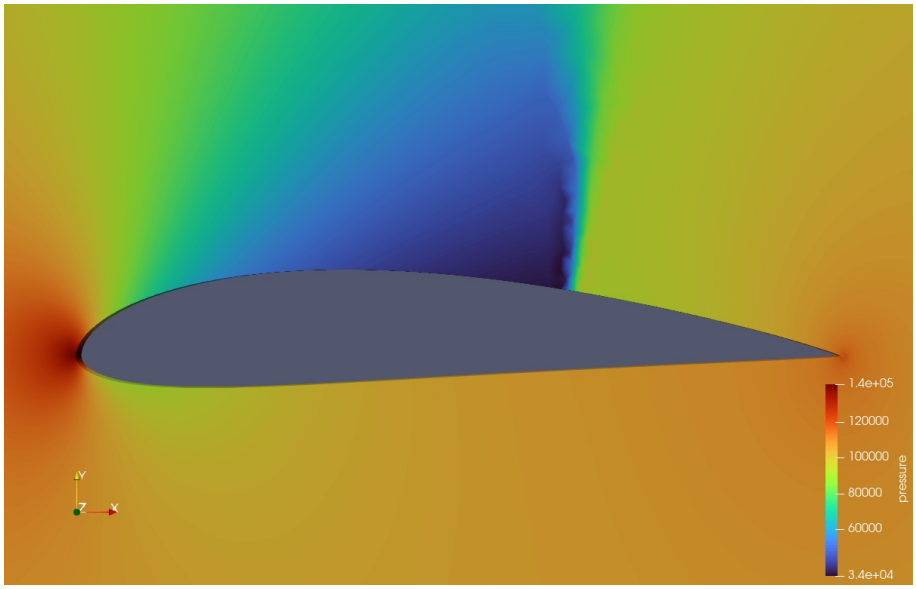

Figure 4.2: *Pressure field around the NACA 4415 airfoil.*

Regression-based ni-PCE

In this subsection, the regression-based ni-PCE method is applied to the NACA 4415 airfoil test case. The objective is to construct stochastic surrogate models for Lift and Drag and to compute their corresponding statistical moments using a limited number of CFD simulations. A total of 15 input samples are generated using Latin Hypercube Sampling (LHS), and the resulting CFD outputs are processed via least-squares regression, as described in Section 2.1.4.

The number of PCE coefficients depends on the chosen chaos order k. For a 2-dimensional input space, the total number of terms is given by:

$$\text{PCE coefficients} = \binom{k+M}{M} = \frac{(k+2)!}{2 \times k!} \tag{4.1}$$

Table 4.2 summarizes the number of PCE coefficients, the Oversampling Ratios (O.R.) (given the 15 CFD runs), and the corresponding results obtained for chaos orders 1, 2, and 3:

Order	Coeffs	O.R.	Lift Mean	Lift Std	Drag Mean	Drag Std
1	3	5	336.611	8.5645	20.2233	1.44415
2	6	2.5	336.55	8.41011	20.2197	1.42251
3	10	1.5	336.575	8.4331	20.2262	1.43739

Table 4.2: *Regression-based ni-PCE results using 20 samples for different chaos orders.*

Order	Lift Mean	Lift Std	Drag Mean	Drag Std
	Rel. Err (%)	Rel. Err (%)	Rel. Err (%)	Rel. Err (%)
1	0.0207	1.8569	0.0289	1.5532
2	0.0025	0.0189	0.0111	0.0304
3	0.0100	0.2926	0.0433	1.0788

Table 4.3: *Relative error (%) of regression-based ni-PCE results with respect to the GQ benchmark.*

As shown in Tables 4.2 and 4.3, the second-order chaos expansion provides the best overall accuracy in estimating the statistical moments of both Lift and Drag. Specifically, the relative errors with respect to the GQ benchmark are below 0.03% for all quantities, indicating excellent agreement. While order 1 underestimates the variability, and order 3 yields slightly less accurate estimates—likely due to the lower oversampling ratio of 1.5 — order 2 strikes the best balance between model complexity and available data in this case. These results highlight the importance of selecting an appropriate chaos order and maintaining a sufficient oversampling ratio to avoid instability in the regression and to ensure accurate moment estimation.

Adjoint-assisted Regression-based ni-PCE

To further reduce the number of required CFD simulations, the adjoint-assisted regression-based ni-PCE approach is employed (see Section 2.1.5). By computing gradients of the QoIs with respect to the uncertain variables using the adjoint method, each sample yields multiple rows in the regression matrix—one from the primal solution and one from each derivative.

For this case, only 4 samples were required. Given that each sample provides $1+2 = 3$ rows, the total number of regression equations is $4 \times 3 = 12$. This allows the construction of a chaos expansion up to order 2, which requires 6 coefficients, and yields an oversampling factor of 2.0.

The results of this analysis are shown in Table 4.4, along with a comparison to the GQ-based benchmark.

QoI	Mean	Rel. Error (%)	Std	Rel. Error (%)
Lift	336.5515	0.0030	8.41102	0.0297
Drag	20.220	0.0126	1.42282	0.0523

Table 4.4: *Adjoint-assisted ni-PCE results using 4 samples (chaos order 2).*

The results in Table 4.4 confirm the remarkable accuracy of the adjoint-assisted ni-PCE method, even when using only 4 CFD simulations. All relative errors remain well below 0.06%, with both the mean and standard deviation of Lift and Drag nearly identical to the high-fidelity GQ-based benchmark. This level of agreement demonstrates the power of incorporating derivative information via the adjoint method, which enriches the regression system and enables accurate surrogate construction with drastically fewer samples. In the context of high-fidelity CFD, where each simulation can be computationally expensive, this efficiency gain is highly significant.

Cost comparison between typical and adjoint-assisted regression

In cases where the evaluation of the QoI is computationally expensive, the efficiency of the regression method becomes questionable. With N_Q evaluations of the QoI and an oversampling factor of r, the cost of the adjoint-assisted regression approach can be expressed as:

$$\text{Cost}_{\text{Adjoint}} = (N_Q + 1)\,\frac{r(M+k)!}{(M+1)!k!}\text{CU}, \tag{4.2}$$

where M is the number of uncertain variables, k is the chaos order, and CU denotes the Cost Unit (i.e. the cost for running the CFD code, usually referred to as an

Equivalent Flow Solution (EFS), if it's a problem in fluid mechanics) of a single QoI evaluation.

Neglecting rounding and assuming exact arithmetic, the ratio of the costs between adjoint-assisted regression and typical regression is approximately:

$$\text{Cost Ratio} = \frac{N_Q + 1}{M + 1}. \tag{4.3}$$

This implies that the adjoint-assisted regression method is more cost-effective in cases where the number of uncertain variables M greater than the number of QoI evaluations N_Q. The inclusion of sensitivity derivatives allows for an increased oversampling factor without additional QoI evaluations, thus reducing the overall computational burden.

However, with number of QoI evaluations N_Q exceeds the number of uncertain variables M, typical regression methods become more favorable due to their simpler implementation and lower computational overhead.

In summary, the adjoint-assisted regression method is advantageous in cases involving a large number of uncertain variables. Conversely, in cases where $N_Q > M$, the typical regression method should be preferred for its efficiency and practicality.

4.2 Case 2: Airfoil Shape Imperfections

In order to demonstrate the application of the Karhunen-Loève expansion in modeling shape imperfections, the n16103 airfoil is used as a test case. The stochastic field representing the imperfections, as mentioned in Section 3.1, is expressed by Equation (3.41).

For computational efficiency, the series is truncated to $N = 18$ terms such that

$$\frac{\sum_{i=1}^{18} \lambda_i}{\sum_{i=1}^{\infty} \lambda_i} \approx 0.95. \tag{4.4}$$

This truncation captures approximately 95% of the total variance, ensuring a balance between accuracy and efficiency in representing manufacturing imperfections. Thus, the uncertainty is fully represented by 18 independent random variables $c_1, c_2, \ldots, c_{18}$ corresponding to the expansion coefficients in Equation (3.41).

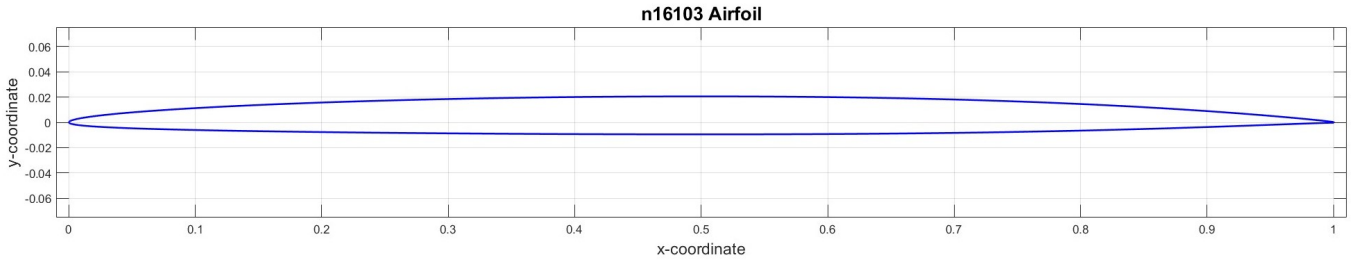

Figure 4.3: *The n16103 airfoil.*

Regression vs GQ PCE

This case is a great example of the advantages of using a regression-based rather than a GQ-based PCE. The total number of simulations required for a GQ-based PCE is given by the following equation:

$$N_{GQ} = (k+1)^M \tag{4.5}$$

where K is the maximum polynomial order and M is the number of stochastic dimensions. This exponential growth in computational cost with increasing dimensionality makes GQ-based PCE infeasible for high-dimensional problems.

In contrast, as already discussed in this thesis, regression-based PCE requires only:

$$N_{reg} = \binom{k+M}{M} \tag{4.6}$$

which grows much slowly with M. For sparse problems, N_{reg} can be further reduced using advanced techniques like least-angle regression (LAR) or compressive sensing.

Thus, in cases like this one, where the number of uncertain variables is significantly larger than the number of QoIs, the regression-based PCE is the only feasible option.

In Figure 4.4, a comparison between the two methods is shown for different chaos orders and uncertain variables.

It is clear that for 18 uncertain variables, the GQ-based PCE is not feasible, as it would require 19.531.441 simulations for a chaos order of 2. In contrast, the regression-based PCE requires only 190 simulations, making it a much more efficient option.

Simulation Parameters

The flows were still simulated using the PUMA software, which solves the Reynolds-Averaged Navier-Stokes (RANS) equations with the Spalart-Allmaras turbulence

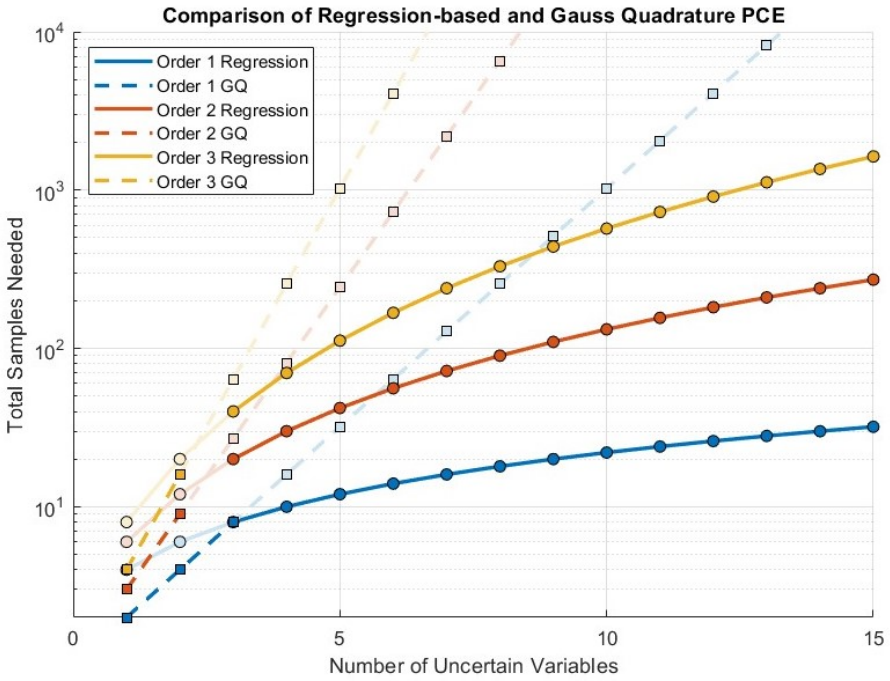

Figure 4.4: *Comparison between regression-based and GQ-based PCE.*

model. A second-order Roe scheme was used for spatial discretization, and time integration was performed using a multi-stage Runge-Kutta method. The solver ran for 30,000 iterations with a CFL number of 10.

The freestream conditions were set to a total pressure of 21,662.72 Pa, a velocity of 252.28 m/s, and a density of 0.3483 kg/m^3. The dynamic viscosity was 2.39824×10^{-5} Pa·s.

The pressure field around the baseline n16103 airfoil (without any imperfections) is shown in Figure 4.5.

The objective of this test case is to quantify the impact of shape imperfections on the aerodynamic performance of the airfoil, specifically in terms of the generated lift and drag. Note that the two QoIs in this problem are the lift and drag. For the 18 uncertain variables in the problem and a chaos expansion of order 2, the total number of PCE coefficients is given by Equation (2.3):

$$\text{PCE coefficients} = \frac{(2+18)!}{2!\cdot 18!} = 190. \tag{4.7}$$

Considering a sufficient oversampling ratio of 3.15 for the PCE, the total number of CFD simulations required is 600. This number can be greatly reduced by using the adjoint method to calculate the gradients of the QoIs with respect to the uncertain variables, as discussed in Section 2.1.5.

Figure 4.5: *Pressure field around the n16103 airfoil.*

Below is the flowchart of the operations performed for each CFD simulation:

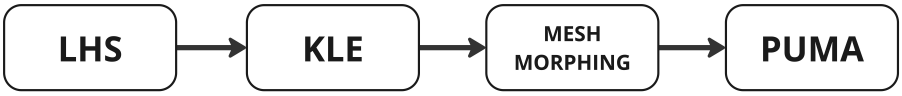

Figure 4.6: *Flowchart of the operations performed for each CFD simulation.*

Firstly, using the LHS technique, a set of 18 random variables is generated, each following a normal distribution with a mean of 0 and a standard deviation of 0.3 (i.e., $\mathcal{N}(0, 0.3^2)$). These random variables are then used to generate the deformed airfoil through the KLE process presented in Section 3.1. Finally, an RBF network is used to adapt the baseline mesh into the deformed airfoil, and the CFD simulation is performed using PUMA.

Benchmark Analysis: ni-PCE Without the Use of the Adjoint

The first step is to establish a benchmark analysis using the ni-PCE method without employing adjoint derivatives, to later compare the results with those obtained using the adjoint method. As described earlier, 600 sets of 18 random variables are generated using the LHS technique, and the corresponding deformed airfoils are produced using the KLE process. Some representative deformed airfoils are shown in Figure 4.7.

The CFD simulations are then performed for each deformed airfoil, and the resulting lift and drag are calculated. The results are processed using the regression-based

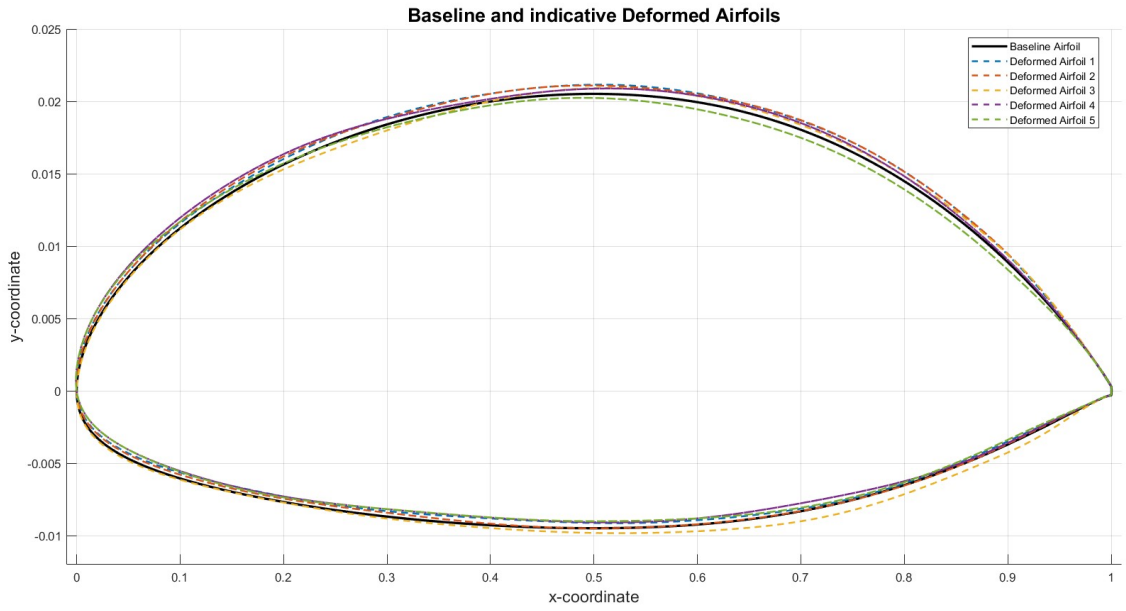

Figure 4.7: *Deformed airfoils generated using the KLE process.*

ni-PCE method, and the stochastic moments of the two QoIs are shown in Table 4.5.

QoI	Mean	Standard Deviation
Lift	2,262.21	93.52
Drag	46.58	1.07

Table 4.5: *Stochastic moments of the QoIs using the ni-PCE method using only responses (no use of gradients).*

Adjoint-assisted ni-PCE

To address the issue of the excessive number of CFD simulations, the adjoint-assisted ni-PCE approach is employed, as described in Section 2.1.5. This approach is highly advantageous, as the number of uncertain variables far exceeds the number of QoIs. For every deformed airfoil, 19 rows of the regression matrix are obtained (one row for the solution of the primal problem, and 18 rows corresponding to the derivatives of the QoIs with respect to the uncertain variables). In this way, the overall computational cost (measured in terms of Equivalent Flow Solutions, EFS) is reduced significantly. Below is a comparison of the number of EFS required for the ni-PCE method without the adjoint and the adjoint-assisted ni-PCE:

As shown in Table 4.6, the adjoint-assisted ni-PCE method significantly reduces the

Method	Deformed Airfoils	Oversampling Ratio	EFS
ni-PCE	600	3.15	600
Adjoint-assisted ni-PCE	50	5.0	100
Adjoint-assisted ni-PCE	30	3.0	60

Table 4.6: *Comparison of methods in terms of Equivalent Flow Solutions (EFS).*

computational cost. Specifically, the number of EFS required for the adjoint-assisted ni-PCE is no more than 10% of that required for the original ni-PCE method, while maintaining the same oversampling ratio. The results obtained from the three cases presented in Table 4.6 are provided in figures 4.7 and 4.8.

Method	Lift Mean [N]	Lift Std [N]	Drag Mean [N]	Drag Std [N]
ni-PCE	2,262.21	93.52	46.58	1.07
Adjoint-assisted ni-PCE (50 airfoils)	2,263.5	91.4	46.52	1.1
Adjoint-assisted ni-PCE (30 airfoils)	2,264.7	89.1	46.45	1.13

Table 4.7: *Stochastic moments of the QoIs (Lift and Drag) for different methods.*

Method	Lift Mean Err (%)	Lift Std Err (%)	Drag Mean Err (%)	Drag Std Err (%)
Adjoint-assisted ni-PCE (50 airfoils)	0.06	-2.27	-0.13	2.8
Adjoint-assisted ni-PCE (30 airfoils)	0.11	-4.73	-0.28	5.6

Table 4.8: *Relative error of each metric with respect to the ni-PCE baseline.*

The results indicate that the adjoint-assisted ni-PCE method closely replicates the baseline ni-PCE outcomes while significantly reducing the computational cost. As shown in Table 4.7, the lift and drag mean values for both the 50-airfoil and 30-airfoil adjoint-assisted cases are nearly identical to the ni-PCE baseline—with relative errors of 0.06% and 0.11% for the lift mean, and -0.13% and -0.28% for the drag mean, respectively.

As expected, the analysis with 50 airfoils exhibits better performance, as it has a larger oversampling ratio and also captures more of the stochastic behavior. Interestingly, the analysis with 30 airfoils also proved to be effective in capturing the mean values of the QoIs very accurately, while struggling a bit more with the standard deviations.

Overall, the adjoint-assisted approach yielded very accurate results, with only 10% of the computational cost of the ni-PCE baseline.

4.3 Case 3: UQ in Supersonic Business Jet Performance Metrics

This section presents a case study on the quantification of uncertainties in the performance metrics of a Supersonic Business Jet (SBJ). The SBJ design is characterized by 12 free variables, encompassing wing parameters, fuel quantity, and geometric features of both the wing and the tail assembly. These variables are summarized in Table 4.9.

Symbol	Variable	Value	Units
M_{cr}	Cruise Mach number	1.8	–
Z_{cr}	Cruise altitude	15,500	m
S_w	Wing area	150	m^2
Λ_{Le}	Leading-edge sweep (wing)	57.5	deg
Λ_{Te}	Trailing-edge sweep (wing)	5	deg
λ_w	Wing taper ratio	0.2750	–
$(t/c)_w$	Max. thickness-to-chord (wing)	0.05	–
$\Lambda_{\text{Le},u}$	Leading-edge sweep (tail)	57.5	deg
$\Lambda_{\text{Te},u}$	Trailing-edge sweep (tail)	5	deg
λ_u	Tail taper ratio	0.275	–
$(t/c)_u$	Max. thickness-to-chord (tail)	0.07	–
W_{fuel}	Fuel weight	22,500	kg

Table 4.9: *Design variables for the SBJ.*

The three performance metrics considered for the SBJ are its range, takeoff length, and approach speed. Before introducing uncertainties in the design variables and performing the UQ analysis, we refer the reader to the mathematical framework for the design presented in Appendix A. The assumed probability distributions, including the mean and standard deviation for each uncertain variable, are summarized in Table 4.10.

Uncertain Variable	Distribution Type	Mean	Standard Deviation
M_{cr}	Normal	1.8	0.025
Z_{cr}	Normal	15,500	312.5
S_w	Normal	150	6.25
Λ_{Le}	Normal	57.5	1.5625
Λ_{Te}	Normal	5	1.25
λ_w	Normal	0.2750	0.0281
$(t/c)_w$	Normal	0.05	0.0012
$\Lambda_{\text{Le},u}$	Normal	57.5	1.5625
$\Lambda_{\text{Te},u}$	Normal	5	1.25
λ_u	Normal	0.275	0.0281
$(t/c)_u$	Normal	0.07	0.0013
W_{fuel}	Normal	22,500	937.5

Table 4.10: *Distribution characteristics of the uncertain design variables.*

Benchmark Analysis: Monte Carlo Simulation

The first step is to perform a benchmark analysis using MC. The goal is to obtain the statistical moments of the performance metrics (range, takeoff length, and approach speed) for the SBJ, which will later serve as a reference for the ni-PCE method. The MC simulation is performed using up to 10^8 samples, ensuring full convergence of the statistical moments. The results are presented in Figure 4.8 and Table 4.11.

Performance Metric	Mean	Standard Deviation
Range (km)	2,786.6	392.07
Takeoff Length (m)	4,154.8	546.337
Approach Speed (m/s)	87.477	3.8516

Table 4.11: *Statistical moments of the performance metrics using MCS.*

Regression-based ni-PCE

As in Case 4.2, the large number of uncertain variables makes a regression-based PCE far more suitable than computing the PCE coefficients via GQ. Specifically, if we were to use a GQ-based PCE with a chaos order of 2, the number of simulations would be:

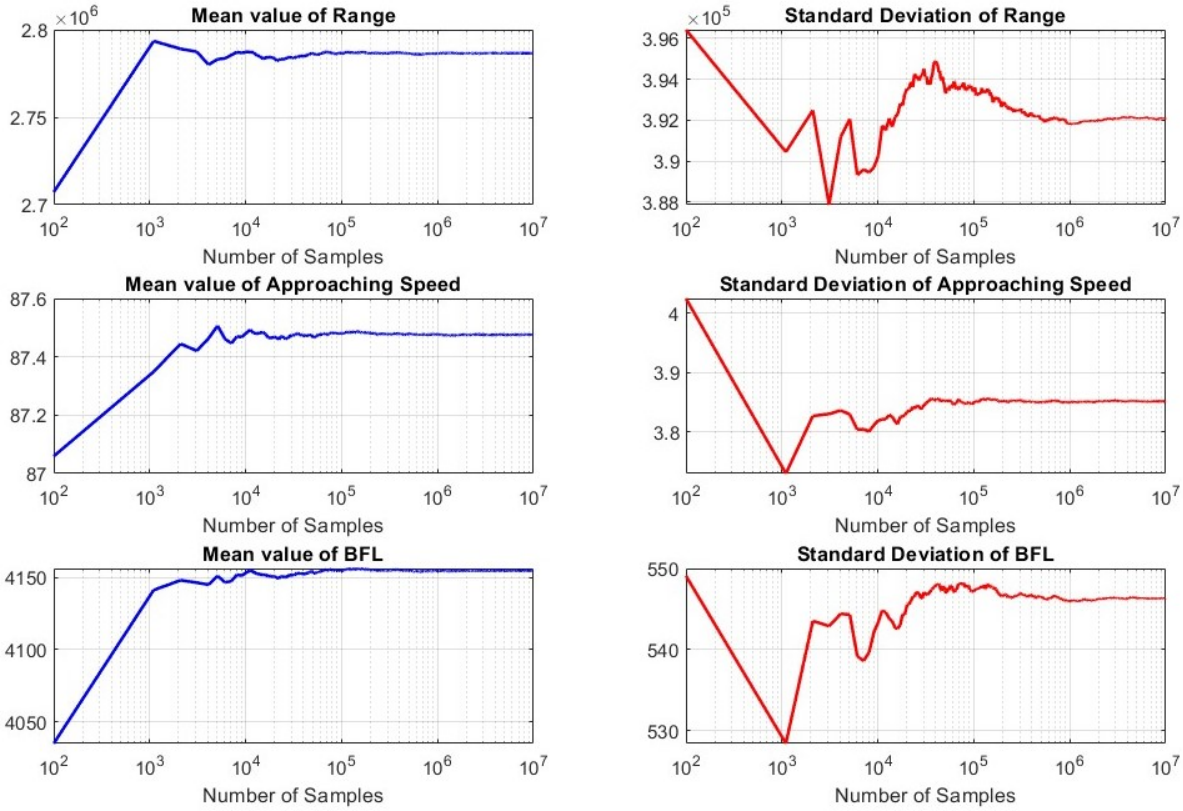

Figure 4.8: *Statistical moments of the performance metrics using different numbers of samples.*

$$\text{Total Samples} = (2+1)^{12} = 531,441$$

In contrast, a regression-based PCE requires significantly fewer samples. Including an oversampling factor of 2, the number of samples required is given by

$$\text{Samples} = 2 \times \binom{12+2}{2} = 2 \times \binom{14}{2} = 2 \times 91 = 182$$

By sampling the uncertain variables from the distributions in Table 4.10, the PCE coefficients can be calculated using regression. The results are presented in Table 4.12.

The results in Table 4.12 show that the regression-based ni-PCE method accurately reproduces the statistical moments of the performance metrics, with relative errors below 1% for all QoIs.

Performance Metric	Mean	Rel. Error (%)	STD	Rel. Error (%)
Range (km)	2,777.8	-0.31	402.55	2.67
Takeoff Length (m)	4,149.2	-0.13	547.21	0.16
Approach Speed (m/s)	87.4906	0.02	3.8531	-0.04

Table 4.12: *Statistical moments of the performance metrics using ni-PCE, including relative errors with respect to MC.*

Gradient-assisted regression-based ni-PCE

To further reduce the total number of samples required for the regression-based ni-PCE, the gradient-assisted approach presented in Section 2.1.5 is employed. In contrast to the previous cases, in which the governing Euler equations were solved and the adjoint method was used to compute the derivatives of the QoIs w.r.t the uncertain variables, the derivatives of the performance metrics in this case are calculated using finite differences—and more specifically, central differencing. Consequently, for each sample, simulations are performed for two additional perturbations of the uncertain variables to compute all derivatives. Although this approach is more expensive than the one presented in subsection 4.3, the objective in this case is to determine whether the gradient information yields accurate results. In typical CFD cases, such as Cases 4.1 and 4.2, the adjoint method would be used to compute the gradients, resulting in a total cost for each sample of approximately 2 EFS. For the needs of the cost comparison, the case will be treated as if the adjoint method was used.

The results obtained using the gradient-assisted regression-based ni-PCE are presented in Table 4.13. To achieve the same oversampling factor of 2 as in the previous case, the total number of samples required is given by

$$\text{Samples} = \frac{\text{oversampling factor} \times \text{PCE coeffs}}{1 + \text{Number of Uncertain Variables}} = \frac{2 \times 91}{1 + 12} = 14 \tag{4.8}$$

Performance Metric	Mean	Rel. Error (%)	STD	Rel. Error (%)
Range (km)	2,775.6	-0.39	399.34	1.85
Takeoff Length (m)	4,148.2	-0.16	544.24	-0.38
Approach Speed (m/s)	87.4981	0.02	3.8732	0.56

Table 4.13: *Statistical moments of the performance metrics using gradient-assisted ni-PCE, including relative errors.*

As shown in Table 4.13, the gradient-assisted regression-based ni-PCE method pro-

duces highly accurate estimates of the statistical moments for the SBJ performance metrics. All relative errors — except for the standard deviation of the range — are within 1%, demonstrating excellent agreement with the benchmark MCS results. When assuming gradient evaluations are obtained via an adjoint method, the total computational cost corresponds to 28 EFS, representing an 84.6% reduction in cost compared to the standard regression-based ni-PCE. This highlights the efficiency and accuracy of incorporating gradient information into the UQ process.

Chapter 5

Conclusions

This diploma thesis has presented a comprehensive investigation into advanced methodologies for UQ in CFD and engineering systems, with a focus on enhancing efficiency and accuracy through adjoint-assisted regression-based PCE and arbitrary PCE frameworks. The work systematically addressed the challenges of quantifying uncertainties in complex high-dimensional systems, particularly those governed by non-standard input distributions and geometric imperfections, while significantly reducing computational costs.

The diploma thesis began by revisiting the foundational ni-PCE method, which treats the computational solver as a black box, avoiding intrusive modifications to governing equations. To improve the regression process, the adjoint method was integrated, leveraging gradient information of the QoI with respect to uncertain inputs. This adjoint-assisted approach formed an overdetermined system using both QoI evaluations and their sensitivities, drastically reducing the number of required CFD simulations, especially for high-dimensional problems. The effectiveness of this method was demonstrated through benchmark problems, such as the Borehole function, where it achieved accurate estimates of stochastic moments with far fewer samples than traditional Monte Carlo simulations.

Recognizing the limitations of classical PCE in handling non-standard input distributions, the thesis adopted,programmed and assesed the aPCE framework. This data-driven approach constructs custom orthogonal polynomial bases tailored to unknown input distributions, utilizing the Mysovskikh theorem and moment-based orthogonalization. The aPCE methodology was rigorously validated, showing its capability to handle arbitrary probability distributions with high accuracy. Specifically, the projection-based aPCE quadrature rule was constructed and validated for up to third-order expansions, using $k + 1 = 4$ nodes per input variable. The generated orthonormal polynomials were verified against known Hermite polynomials in the Gaussian case, with relative errors of the nodes and polynomial coefficients

below 10^{-3}. The accuracy of the constructed quadrature was assessed using a 2-D benchmark function for which the aPCE quadrature computed a mean and a standard deviation with relative errors on the order of 10^{-4}. Also, the same framework was applied to a 2-D problem with unknown input distributions, yielding similar accuracy. These results confirm the robustness and precision of the aPCE methodology, making it suitable for a wide range of real-world UQ problems involving non-standard inputs. Additionally, the KLE was employed to model geometric shape imperfections, providing a compact and mathematically consistent representation of random fields such as manufacturing deviations.

A comprehensive comparison is summarized in Table 5.1, presenting statistical metrics—mean and standard deviation—along with relative errors and computational costs (expressed in equivalent flow solutions, EFS). The results demonstrate that the adjoint-assisted regression-based PCE significantly outperforms traditional regression-based PCE and Monte Carlo Simulation (MCS) in terms of cost-efficiency, especially in high-dimensional settings.

Method	**QoI**	**Mean**	**Error Mean (%)**	**Std. Dev.**	**Error Std. Dev. (%)**	**Cost (EFS)**
Case Study 1: NACA 4415 (2 Uncertain Variables)						
GQ-PCE	Lift	336.54131	-	8.40852	-	9
GQ-PCE	Drag	20.21745	-	1.42208	-	9
Reg-PCE (order 2)	Lift	336.55	0.0025	8.41011	0.0189	15
Reg-PCE (order 2)	Drag	20.2197	0.0111	1.42251	0.0304	15
Adjoint-Reg-PCE	Lift	336.55	0.003	8.411	0.03	4
Adjoint-Reg-PCE	Drag	20.22	0.0126	1.4282	0.0523	4
Case Study 2: n16103 (18 Uncertain Variables)						
Reg-PCE	Lift	2262.2	-	93.52	-	600
Reg-PCE	Drag	46.58	-	1.07	-	600
Adjoint-PCE (50 samples)	Lift	2263.5	0.06	91.4	-2.27	100
Adjoint-PCE (50 samples)	Drag	46.52	-0.13	1.10	2.80	100
Adjoint-PCE (30 samples)	Lift	2264.7	0.11	89.1	-4.73	60
Adjoint-PCE (30 samples)	Drag	46.45	-0.28	1.13	5.60	60
Case Study 3: SBJ (12 Uncertain Variables)						
MCS	Range	2786.6	-	392.1	-	10^8
MCS	Takeoff	4154.8	-	546.3	-	10^8
MCS	Approach	87.477	-	3.852	-	10^8
Reg-PCE	Range	2777.8	-0.31	402.6	2.67	182
Reg-PCE	Takeoff	4149.2	-0.13	547.2	0.16	182
Reg-PCE	Approach	87.491	0.02	3.853	-0.04	182
Grad-Reg-PCE	Range	2775.6	-0.39	399.3	1.85	28
Grad-Reg-PCE	Takeoff	4148.2	-0.16	544.2	-0.38	28
Grad-Reg-PCE	Approach	87.498	0.02	3.873	0.56	28

Table 5.1: *Quantitative comparison of UQ methods for the studied case studies.*

In the 2D airfoil problem (NACA 4415), the adjoint-regression method reduced the cost by more than 70% (from 15 to 4 EFS) while maintaining sub-0.05% errors in

mean and standard deviation compared to GQ-based PCE.

In the 18-dimensional case (n16103 airfoil), the adjoint-assisted PCE achieved similar or better accuracy than classical regression PCE, with only 50 or even 30 samples. This corresponds to an 83%–90% reduction in cost, at the expense of only 0.06%–0.11% error in the mean and up to 5.6% in standard deviation.

For the Supersonic Business Jet case (12 uncertain variables and chaos order 2), where full Monte Carlo simulation required 100 million calls to the evaluation software, the gradient- assisted PCE achieved comparable accuracy (within $\pm 0.5\%$ in both mean and standard deviation) at a cost that is 6 orders of magnitude lower (28 EFS vs. 10^8).

In conclusion, this thesis explored the integration of adjoint sensitivity information and unknown distribution in handling polynomial chaos methods, as well as the aPCE framework for unknowwn distributions, extending their applicability to a broader range of real-world CFD problems. The methodologies developed herein provide a scalable and efficient framework for UQ, balancing accuracy with computational feasibility.

Appendix A

Supersonic Business Jet Mathematical Framework

The SBJ can be divided into seven main disciplines, each with its own set of inputs and outputs. The outputs of one discipline may serve as the inputs of another, forming a coupled system that must be solved iteratively. These kinds of problems are referred to as Multi-Disciplinary Analysis (MDA) problems.

This first discipline addresses the operational conditions during flight. Its inputs are the cruise altitude z_{cr} and cruise Mach number M_{cr}, while the outputs consist of the ambient pressure p_{cr}, air density ρ_{cr}, temperature T_{cr}, and the aircraft's flight speed V_{cr}.

To compute these outputs, a standard (piecewise) atmospheric model is used. First, the temperature at the flight altitude is approximated by:

$$T_{\text{cr}} = \begin{cases} T_0 - B\, z_{\text{cr}}, & \text{for } z_{\text{cr}} \leq 11{,}000\,\text{m} \\ 216.65, & \text{for } 11{,}000 < z_{\text{cr}} \leq 10{,}000\,\text{m} \end{cases} \tag{A.1}$$

where T_0 is the sea-level temperature, and $B = -\frac{dT}{dz} = 0.0065\,\text{K/m}$ is the atmospheric lapse rate.

Next, the pressure at altitude is computed by a corresponding piecewise function:

$$p_{\mathrm{cr}} \;=\; \begin{cases} p_0\Big(1 - \dfrac{B\, z_{\mathrm{cr}}}{T_0}\Big)^{\frac{g}{R\,B}}, & \text{for } z_{\mathrm{cr}} \le 11{,}000\,\mathrm{m} \\ p_{11}\, \exp\Big(-\dfrac{g}{R\,T_{\mathrm{cr}}}(\, z_{\mathrm{cr}} - z_{11}\Big), & \text{for } 11{,}000 < z_{\mathrm{cr}} \le 10{,}000\,\mathrm{m} \end{cases} \tag{A.2}$$

where $g = 9.81\,\mathrm{m/s^2}$ is the gravitational acceleration, $R = 287.04\,\mathrm{J/(kg{\cdot}K)}$ is the specific gas constant for air, p_0 is the known pressure at sea level, and p_{11} is the pressure at 11,000 m.

The air density at altitude is then obtained via the ideal-gas law:

$$\rho_{\mathrm{cr}} = \begin{cases} \rho_0 \left(\dfrac{T_{\mathrm{cr}}}{T_0}\right)^{\frac{g}{R\,B}-1}, & z_{\mathrm{cr}} \le 11000, \\ \dfrac{p_{\mathrm{cr}}}{R\,T_{\mathrm{cr}}}, & 11000 < z_{\mathrm{cr}} \le 10000, \end{cases} \tag{A.3}$$

where ρ_0 is the air density at ground level.

Finally, the flight speed V_{cr} can be computed from the Mach number and the temperature as:

$$V_{\mathrm{cr}} = M_{\mathrm{cr}}\, \sqrt{\gamma\, R\, T_{\mathrm{cr}}}, \tag{A.4}$$

where $\gamma = 1.4$ is the ratio of specific heats for air.

The second aspect regards the fuselage geometry, which is idealized as a cylindrical body capped with cones at both ends. The diameter of the fuselage is fixed at $D_f = 2.15\,\mathrm{m}$. The front cone is assumed to lie within the Mach cone, while the rear cone has a known half-angle of 12°.

The two input parameters to this discipline are the cruise Mach number M_{cr} and the takeoff fuel weight W_{fuel}, while the outputs are the total fuselage length L_f and its outer surface area S_f.

The overall fuselage length is expressed as the sum of four sections:

$$L_f = L_{f1} + L_{f2} + L_{f3} + L_{f4} \tag{A.5}$$

where:

- L_{f1} is the front cone length,

- L_{f2} is the rear cone length,

- L_{f3} is the cabin/passenger section length,

- L_{f4} is the fuel section length.

The front cone length depends on the Mach number and is given by:

$$L_{f1} = 0.5 D_f \left(\tan \left(0.3 \arcsin \left(\frac{1}{M_{\text{cr}}} \right) \right) \right)^{-1}, \tag{A.6}$$

while the rear cone length is based on its fixed cone angle:

$$L_{f2} = 0.5 D_f \left(\tan(12^\circ) \right)^{-1}. \tag{A.7}$$

The passenger section is assumed to be a fixed length:

$$L_{f3} = 10\,\text{m}. \tag{A.8}$$

The fuel section length is computed from the fuel volume at takeoff, which is determined from the fuel weight and density:

$$L_{f4} = \frac{V_{\text{fuel}}}{\frac{\pi}{4} D_f^2}, \quad \text{where } V_{\text{fuel}} = \frac{W_{\text{fuel}}}{\rho_{\text{fuel}}}, \tag{A.9}$$

with $\rho_{\text{fuel}} = 807.5\,\text{kg/m}^3$.

Finally, the total surface area of the fuselage is given by:

$$S_f = \pi D_f \left(L_{f3} + L_{f4} + 0.5 \left(\sqrt{\frac{D_f^2}{4} + L_{f1}^2} + \sqrt{\frac{D_f^2}{4} + L_{f2}^2} \right) \right). \tag{A.10}$$

The next discipline focuses on modeling the geometry of the aircraft's wing. The input parameters for this discipline include the wing surface area S_w, the leading-edge sweep angle $\Lambda_{w,LE}$, the trailing-edge sweep angle $\Lambda_{w,TE}$, the thickness-to-chord ratio $\left(\frac{t}{c}\right)_w$, and the tip-to-root chord ratio λ_w.

The outputs from this model are the mean wing chord c_{rw}, the span b_w, the aspect ratio AR_w, the sweep angle at the quarter-chord location $\Lambda_{w,25}$, the exposed wing surface area $S_{w,\text{exp}}$, and the wetted wing surface area $S_{w,\text{wet}}$.

The mean aerodynamic chord is calculated using the following equation:

$$c_{rw} = \sqrt{\frac{S_w \left(\tan \Lambda_{w,LE} - \tan \Lambda_{w,TE} \right)}{1 - \lambda_w^2}} \tag{A.11}$$

The wing span is then given by:

$$b_w = \frac{2S_w}{c_{rw}(1+\lambda_w)} \tag{A.12}$$

From the span and surface area, the aspect ratio is computed as:

$$AR_w = \frac{b_w^2}{S_w} \tag{A.13}$$

The exposed surface area is calculated by removing the fuselage-interfered portion of the wing planform:

$$S_{w,\text{exp}} = S_w - \frac{D_f}{2}\left(2c_{rw} - \frac{D_f}{2}\tan\Lambda_{w,LE} + \frac{D_f}{2}\tan\Lambda_{w,TE}\right) \tag{A.14}$$

The discipline of th vertical stabilizer geometry closely resembles the wing geometry model. The input variables for this discipline are: the wing surface area S_w, the sweep angle at the leading edge $\Lambda_{v,LE}$, the sweep angle at the trailing edge $\Lambda_{v,TE}$, the thickness-to-chord ratio $\left(\frac{t}{c}\right)_v$, and the tip-to-root chord ratio λ_v.

The outputs of the discipline include the surface area of the vertical stabilizer S_v, the height b_v, the mean aerodynamic chord c_{rv}, the sweep angle at the 25% chord line $\Lambda_{v,25}$, and the wetted area $S_{v,\text{wet}}$.

The vertical stabilizer surface area is assumed to be 10% of the wing surface area:

$$S_v = 0.1\, S_w \tag{A.15}$$

The mean chord of the vertical stabilizer is computed similarly to the wing:

$$c_{rv} = \sqrt{\frac{S_v\left(\tan\Lambda_{v,LE} - \tan\Lambda_{v,TE}\right)}{1-\lambda_v^2}} \tag{A.16}$$

The height of the vertical stabilizer is derived from:

$$b_v = \frac{2S_v}{c_{rv}(1-\lambda_v)} \tag{A.17}$$

Finally, the wetted surface area of the vertical stabilizer is estimated as:

$$S_{v,\text{wet}} = 2\left(1 + 0.2\left(\frac{t}{c}\right)_v\right) S_v \tag{A.18}$$

The next discipline addresses both the operation and geometric sizing of the aircraft's engines. The input parameters include all relevant flight condition variables—namely, cruise altitude z_{cr}, Mach number M_{cr}, temperature T_{cr}, pressure p_{cr}, density ρ_{cr}, and velocity V_{cr}. Additional inputs include the wing surface area S_w and the drag coefficient C_D.

The outputs from this discipline are the engine power during flight P, the engine power at ground level P_0, the specific fuel consumption sfc, the nacelle length L_{nac}, and the nacelle diameter D_{nac}.

The power produced by the engine in flight is given by:

$$P = \frac{1}{N_{\text{engine}}} \cdot \frac{1}{2}\rho_{\text{cr}} V_{\text{cr}}^2 C_D S_w \tag{A.19}$$

where $N_{\text{engine}} = 2$ is the number of engines on the aircraft.

If the flight power P is known, the power at sea level is estimated using:

$$P_0 = P\left(0.6\frac{p_{\text{cr}}}{p_0}\left(1 + \frac{\gamma - 1}{2}M_{\text{cr}}^2\right)^{\frac{\gamma}{\gamma - 1}}\right) \tag{A.20}$$

The specific fuel consumption is calculated using:

$$sfc = 2.8310^{-5}(0.9 + 0.3M_{\text{cr}})\sqrt{\frac{T_{\text{cr}}}{T_0}}, \tag{A.21}$$

To determine nacelle size, the engine diameter and length must be calculated first. These depend on the power at ground level P_0 as follows:

$$D_{\text{engine}} = c_1 P_0^{k_1}, \qquad L_{\text{engine}} = c_2 P_0^{k_2} \tag{A.22}$$

where the constants are:

$$c_1 = 0.0062, \quad k_1 = 0.67, \quad c_2 = 0.025, \quad k_2 = 0.46$$

The nacelle length is then determined by:

$$L_{\text{nac}} = 4D_{\text{engine}} + L_{\text{engine}} \tag{A.23}$$

and the nacelle diameter is:

$$D_{\text{nac}} = 1.1 D_{\text{engine}} \tag{A.24}$$

The next discipline is responsible for computing the aircraft's total weight. The required input variables include: the wing geometry parameters S_w, $\left(\frac{t}{c}\right)_w$, $\Lambda_{w,25}$, b_w, λ_w, and $S_{w,\text{exp}}$; the vertical stabilizer parameters S_v, b_v, $\left(\frac{t}{c}\right)_v$, and $\Lambda_{v,25}$; fuselage parameters S_f and L_f; atmospheric pressure at cruise altitude p_{cr}; engine power at sea level P_0; and the fuel weight at takeoff W_{fuel}.

The two outputs from this discipline are the total takeoff weight TOW and the zero-fuel weight ZFW.

The total weight is calculated as the sum of the zero-fuel weight and the takeoff fuel weight:

$$TOW = ZFW + W_{\text{fuel}} \tag{A.25}$$

The zero-fuel weight is composed of payload and crew weight, operational weight, and the empty aircraft weight:

$$ZFW = W_{\text{payload}} + W_{\text{crew}} + W_{\text{operational}} + W_{\text{empty}} \tag{A.26}$$

The payload and crew weights are approximated by:

$$W_{\text{payload}} + W_{\text{crew}} = (N_{\text{passengers}} + N_{\text{crew}}) W_{\text{person}} = (12 + 3) \times 100 = 1500 \tag{A.27}$$

A fixed value is assumed for operational weight:

$$W_{\text{op}} = 210 kg \tag{A.28}$$

The empty weight is the sum of individual components:

$$W_{\text{empty}} = W_w + W_v + W_f + W_{\text{gear}} + W_{\text{fe}} + N_{\text{engine}} W_{\text{engine}} \tag{A.29}$$

The wing weight is given by:

$$W_w = 20.6\, S_w \;+\; 5.387 \times 10^{-6} \times \frac{4.5\, b_w^3 \sqrt{TOW \;\; ZFW}\, \left(1 + 2\,\lambda_w\right)}{\left(\frac{t}{c}\right)_w \cos^2\!\left(\Lambda_{w,25}\right) S_{w,\text{exp}} \left(1 + \lambda_w\right)} \tag{A.30}$$

Similarly, the vertical stabilizer weight is estimated as:

$$W_v = 12.8\, S_v + 24 \times 10^{-6} \frac{b_v^3 \left(8 + 0.09 \frac{TOW}{S_{w,\exp}}\right)}{\left(\frac{t}{c}\right)_v \cos \Lambda_{v,25}{}^2} \tag{A.31}$$

The fuselage weight is calculated using:

$$W_f = (5.1314 + 0.498\, I_f)\, S_f, \tag{A.32}$$

where the index I_f is computed as:

$$I_f = \begin{cases} I_p & \text{if } I_p > I_b, \\ \frac{I_p + I_b}{2} & \text{if } I_p \leq I_b, \end{cases} \tag{A.33}$$

with the pressure index given by:

$$I_p = 10^{-4}(p_{\text{cr}} - p_{\text{cabin}}) D_f \tag{A.34}$$

and the buckling index defined as:

$$I_b = 1.3 \times 10^{-4} \frac{4.5\, W_f\, L_f}{D_f^2} \tag{A.35}$$

The remaining terms are calculated as follows:

$$W_t = ZFW - W_w - N_{\text{engine},w} W_{\text{engine}} \tag{A.36}$$

where $N_{\text{engine},w}$ is the number of engines attached to the wing. The engine weight is estimated via:

$$W_{\text{engine}} = 3.5 \times 10^{-2} P_0^{0.9255} \tag{A.37}$$

and the weights of the gear and flight electronics are modeled as fractions of the takeoff weight:

$$W_{\text{gear}} = 0.04\, TOW, \qquad W_{\text{fe}} = 0.08\, TOW \tag{A.38}$$

The aerodynamics discipline is responsible for evaluating the aircraft's aerodynamic performance, specifically by computing the lift and drag coefficients.

The input parameters to this discipline include the wing geometry variables S_w, $S_{w,\text{wet}}$, c_{rw}, $\left(\frac{t}{c}\right)_w$, b_w, λ_w, $\Lambda_{w,LE}$, and AR_w; the vertical stabilizer geometry variables S_v, $S_{v,\text{wet}}$, c_{rv}, $\left(\frac{t}{c}\right)_v$, b_v, and λ_v; the fuselage geometry parameters L_f and S_f; the nacelle length and diameter L_{nac}, D_{nac}; the flight condition variables M_{cr}, T_{cr}, ρ_{cr}, V_{cr}; and the total weight at takeoff TOW.

The outputs of this discipline are the lift coefficient C_L and drag coefficient C_D.

The lift force is calculated from:

$$L = 0.5\,\rho_{\text{cr}}\,V_{\text{cr}}^2\,S_w \tag{A.39}$$

Assuming that the lift equals 95% of the total aircraft weight in flight:

$$C_L = \frac{0.95\,g\,TOW}{0.5\,\rho_{\text{cr}}\,V_{\text{cr}}^2\,S_w} \tag{A.40}$$

The drag coefficient is the sum of parasitic drag and lift-induced drag:

$$C_D = C_{D,0} + C_{D,i} \tag{A.41}$$

The induced drag is calculated using:

$$C_{D,i} = K\,C_L^2 \tag{A.42}$$

The value of K depends on the Mach number and is defined as:

$$K = \begin{cases} \frac{1}{\pi\,AR_w\,e} & M_{\text{cr}} < 1 \\ \frac{AR_w\,(M_{\text{cr}}^2-1)}{4\,AR_w + (M_{\text{cr}}^2-1)\cos\Lambda_{w,LE}} & M_{\text{cr}} \geq 1 \end{cases} \tag{A.43}$$

where e is the Oswald efficiency factor given by:

$$e = 4.61\left(1 - 0.045\,AR_w^{0.68}\right)\left(\cos\Lambda_{w,LE}\right)^{0.15} - 3.1 \tag{A.44}$$

The parasitic drag coefficient depends on Mach number:

$$C_{D,0} = \begin{cases} C_{D,\text{visc}} + C_{D,\text{gear}} & M_{\text{cr}} < 1 \\ C_{D,\text{visc}} + C_{D,\text{wave}} & M_{\text{cr}} \geq 1 \end{cases} \tag{A.45}$$

The wave drag coefficient is calculated by:

$$C_{D,\text{wave}} = \frac{9\pi}{2S_w}\left(\frac{A_{\max}}{L_f}\right)^2 E_{\text{wd}}\left(1 - 0.386(M_{\text{cr}} - 1.2)^{0.57}\left(1 - \frac{\pi\,\Lambda_{w,LE}}{100}\right)\right) \quad \text{(A.46)}$$

where $E_{\text{wd}} = 2$ and $A_{\max}$ is the maximum frontal area.

The viscous drag is the sum of the friction drag over all wetted surfaces:

$$C_{D,\text{visc}} = \sum_i \frac{S_{i,\text{wet}}}{S_i} c_{f,i} \quad \text{(A.47)}$$

Each surface friction coefficient $c_{f,i}$ is computed as:

$$c_{f,i} = \frac{0.074}{Re_{t,i}^{0.2}} \frac{r_t^2}{r_R} \quad \text{(A.48)}$$

The "wall" temperature is calculated:

$$T_w = T_{\text{cr}}(1 + 0.178M_{\text{cr}}^2) \quad \text{(A.49)}$$

Air viscosity is computed using:

$$\mu = 17.15 \times 10^{-6}\left(\frac{T_w}{273.0}\right)^{1.5} \frac{273 + 110.4}{T_w + 110.4} \quad \text{(A.50)}$$

The correction factors are:

$$r_R = 1.0 + 0.1151M_{\text{cr}}^2 \quad \text{(A.51)}$$

$$r_T = 0.5(1.0 + r_T)r_R^{1.5} \quad \text{(A.52)}$$

The Reynolds number is given by:

$$Re_{t,i} = \frac{\rho_{\text{cr}} V_{\text{cr}} L_{\text{char}}}{\mu} \quad \text{(A.53)}$$

The characteristic length L_{char} for each surface is:

- L_{nac} for the nacelle,
- L_f for the fuselage,
- $c_{i,\text{mean}}$ for the wing and vertical stabilizer.

The mean chord for surface i is calculated as:

$$c_{i,\text{mean}} = \frac{2\, c_{r,i}\, (1 + \lambda_i + \lambda_i^2)}{3\, (1 + \lambda_i)} \tag{A.54}$$

In Figure A.1, a flowchart of the MDA process is presented.

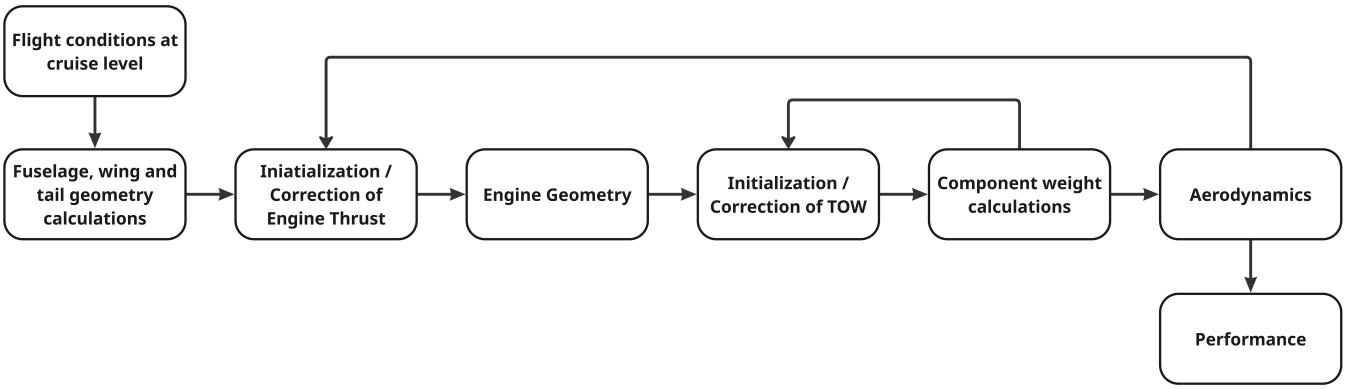

Figure A.1: *Flowchart of the MDA process for the Supersonic Business Jet.*

Bibliography

[1] Abramowitz, M., Stegun, I.A.: Handbook of Mathematical Functions with Formulas, Graphs, and Mathematical Tables. Dover Publications, New York (1972)

[2] Asouti, V., Trompoukis, X., Kampolis, I., Giannakoglou, K.: Unsteady CFD computations using vertex–centered finite volumes for unstructured grids on Graphics Processing Units. International Journal for Numerical Methods in Fluids **67**(2), 232–246 (May 2011)

[3] Avdonin, A.: Local modeling and uncertainty quantification of the linear flame response. Ph.d. dissertation, Technische Universität München, Munich, Germany (Feb 2022)

[4] Avelino, J.G., Cavalcanti, G.D.C., Cruz, R.M.O.: Resampling strategies for imbalanced regression: A survey and empirical analysis. Artificial Intelligence Review **57**, 82 (2024). https://doi.org/10.1007/s10462-024-10724-3, https://doi.org/10.1007/s10462-024-10724-3

[5] Eldred, M.S.: Recent advances in non-intrusive polynomial chaos and stochastic collocation methods for uncertainty analysis and design. American Institute of Aeronautics and Astronautics Paper (2009–2274) (2009)

[6] Eldred, M.S., Webster, C.G., Constantine, P.G.: Evaluation of non-intrusive approaches for wiener-askey generalized polynomial chaos (2008), american Institute of Aeronautics and Astronautics Paper 2008–1892

[7] Gander, W.: The singular value decomposition (2008)

[8] Ghanem, R.G., Spanos, P.D.: Stochastic Finite Elements: A Spectral Approach. Dover Publications, New York, revised edn. (2003)

[9] Grigoriu, M.: Stochastic Calculus: Applications in Science and Engineering. Birkhauser, Boston (2002)

[10] Li, H., Zhang, D.: Probabilistic collocation method for flow in porous media: Comparisons with other stochastic methods. Water Resources Research **43**, 44–48 (2009)

[11] Lumley, J.L.: The structure of inhomogeneous turbulent flows. In: Yaglom, A.M., Tatarski, V.I. (eds.) Atmospheric Turbulence and Wave Propagation, pp. 166–178 (1967)

[12] Marelli, S., Sudret, B.: Uqlab user manual - polynomial chaos expansions. Tech. rep., Chair of Risk, Safety & Uncertainty Quantification, ETH Zurich (2015)

[13] Mysovskikh, I.P.: On the construction of cubature formulas with the smallest number of nodes. Doklady Akademii Nauk SSSR **178**(6), 1252–1254 (1968), http://www.mathnet.ru/eng/agreement

[14] Oladyshkin, S., Nowak, W.: Data-driven uncertainty quantification using the arbitrary polynomial chaos expansion. Reliability Engineering and System Safety **106**, 179–190 (2012). https://doi.org/10.1016/j.ress.2012.05.002, http://www.elsevier.com/locate/ress

[15] Papoutsis-Kiachagias, E., Asouti, V., Giannakoglou, K.: Assessment of variants of the method of moments and polynomial chaos approaches to aerodynamic uncertainty quantification. Uncertainty Quantification in Computational Sciences and Engineering **4**(1), 1–20 (Jun 2021)

[16] Pearson, K.: On lines and planes of closest fit to systems of points in space. Philosophical Magazine **2**(6), 559–572 (1901)

[17] Saracco, P., Batic, M., Hoff, G., Pia, M.G.: Uncertainty quantification (uq) in generic montecarlo simulations. IEEE Transactions on Nuclear Science pp. 2805–2813 (2012)

[18] Schober, P., Boer, C., Schwarte, L.A.: Correlation coefficients: Appropriate use and interpretation. Anesthesia & Analgesia **126**(5), 1763–1768 (2018). https://doi.org/10.1213/ANE.0000000000002864, https://www.researchgate.net/publication/323388613_Correlation_Coefficients_Appropriate_Use_and_Interpretation

[19] Silverman, B.W.: Density Estimation for Statistics and Data Analysis. Chapman and Hall, London (1986)

[20] Surjanovic, S., Bingham, D.: Borehole function (2024), https://uqtestfuns.readthedocs.io/en/stable/test-functions/borehole.html

[21] Trefethen, L.N., Bau, D.: Numerical Linear Algebra. SIAM, Philadelphia (1997)

[22] Varah, J.M.: Positive definite hankel matrices of minimal condition. Elsevier Science Inc (2003)

[23] Villete, S.: Advanced techniques in polynomial chaos and bayesian inference for uncertainty quantification (2022)

[24] Γ. Πάμπαλης: Υλοποίηση Αναπτύγματος Πολυωνυμικού Χάους στον Αεροδυναμικά Στιβαρό Σχεδιασμό, Βελτιστοποίηση με Εξελικτικούς Αλγορίθμους υπό Στοχαστικές Εισόδους (2022)

Εθνικό Μετσόβιο Πολυτεχνείο
Σχολή Μηχανολόγων Μηχανικών
Τομέας Ρευστών
Μονάδα Παράλληλης Υπολογιστικής Ρευστοδυναμικής
& Βελτιστοποίησης

Ποσοτικοποίηση Αβεβαιότητας μέσω (Αυθαίρετου) Πολυωνυμικού Αναπτύγματος Χάους με χρήση Γραμμικής Παλινδρόμησης και της Συζυγούς Μεθόδου

Διπλωματική Εργασία

Ιωάννης Λύρας

Επιβλέποντες:
Κυριάκος Χ. Γιαννάκογλου, Καθηγητής ΕΜΠ
Δρ. Β. Ασούτη, Εντεταλμένη Διδάσκουσα ΕΜΠ

Αθήνα, 2025

Περιεχόμενα

Κεφάλαιο 1

Εισαγωγή

Η Ποσοτικοποίηση Αβεβαιοτήτων (Uncertainty Quantification - UQ) αποτελεί βασικό πεδίο της υπολογιστικής επιστήμης, καθώς επικεντρώνεται στη διάδοση των αβεβαιοτήτων εισόδου μέσα από μη-γραμμικά συστήματα με σκοπό την αποτίμηση της επίδρασής τους στην έξοδο. Οι αβεβαιότητες αυτές μπορεί να προέρχονται από φυσική μεταβλητότητα, σφάλματα μέτρησης ή προσεγγίσεις μοντελοποίησης. Οι έξοδοι των συστημάτων αυτών ονομάζονται Ποσότητες Ενδιαφέροντος (Quantities of Interest - QoIs).

Μία από τις βασικές τεχνικές στην ποσοτικοποίηση αβεβαιοτήτων είναι η προσομοίωση Monte Carlo [5], μια στατιστική μέθοδος που βασίζεται στη δειγματοληψία για την εκτίμηση της κατανομής του QoI. Ωστόσο, η μέθοδος αυτή απαιτεί μεγάλο πλήθος δειγμάτων για αξιόπιστα αποτελέσματα. Για τον σκοπό αυτό, εφαρμόζονται παραλλαγές του Πολυωνυμικού Αναπτύγματος Χάους (Polynomial Chaos Expansion - PCE) [2], το οποίο εκφράζει τις QoIs ως ανάπτυγμα ορθοκανονικών πολυωνύμων επί των τυχαίων εισόδων.

Ιδιαίτερο ενδιαφέρον παρουσιάζει το μη επεμβατικό PCE (ni-PCE) [1], το οποίο μεταχειρίζεται το υπολογιστικό μοντέλο ως μαύρο κουτί. Επιπλέον, στη μέθοδο γραμμικής παλινδρόμησης [4], ενσωματώνονται και οι ευαισθησίες των ποσοτήτων ενδιαφέροντος μέσω της συζυγούς μεθόδου, μειώνοντας σημαντικά τον απαιτούμενο αριθμό δειγμάτων. Πέραν των τυποποιημένων κατανομών εισόδου, το Arbitrary PCE (aPCE) [3] επιτρέπει την κατασκευή πολυωνυμικής βάσης προσαρμοσμένης σε εμπειρικές ή άγνωστες κατανομές, ενισχύοντας την ευελιξία και ακρίβεια της μεθόδου.

Η διπλωματική αυτή εργασία επικεντρώνεται στην ανάπτυξη και αξιολόγηση αποδοτικών τεχνικών UQ στο πλαίσιο της Υπολογιστικής Ρευστοδυναμικής (Computational Fluid Dynamics - CFD), με εφαρμογή σε προβλήματα με αβεβαιότητες στη ροή γύρω από αεροτομές, ατέλειες σχήματος και επιδόσεις υπερηχητικού αεροσκάφους, καταδεικνύοντας τη μείωση κόστους χωρίς απώλεια ακρίβειας.

Κεφάλαιο 2

Πολυωνυμικό Ανάπτυγμα Χάους

Το Πολυωνυμικό Ανάπτυγμα Χάους εκφράζει στοχαστικές ποσότητες ενδιαφέροντος ως ανάπτυγμα:

$$\mathrm{J}(\vec{c}) \approx \sum_{i=0}^{Q-1} \alpha_i H_i(\vec{c}), \tag{2.1}$$

όπου $\vec{c}$ είναι οι αβέβαιες μεταβλητές εισόδου, H_i ορθογωνικά πολυώνυμα βάσης και α_i οι συντελεστές του αναπτύγματος. Το πλήθος των όρων Q ορίζεται συναρτήσει των αβέβαιων μεταβλητών M και της τάξης k του αναπτύγματος ως:

$$Q = \frac{(M+k)!}{M!k!} \tag{2.2}$$

Η τάξη χάους k προσδιορίζει το μέγιστο βαθμό των πολυωνύμων βάσης.

2.1 Μη Επεμβατικό PCE

Το μη επεμβατικό Πολυνωνυμικό Ανάπτυγμα Χάους ni-PCE επιτρέπει την προσεγγιστική αναπαράσταση της ποσότητας ενδιαφέροντος, χωρίς παρέμβαση στις μαθηματικές εξισώσεις που διέπουν το σύστημα.

2.1.1 Γραμμική Παλινδρόμηση (Regression)

Στη μέθοδο της γραμμικής παλινδρόμησης, αρχικά επιλέγεται ένα σύνολο N δειγμάτων από το πεδίο ορισμού των αβέβαιων μεταβλητών $\vec{c}$ με μεθόδους όπως η LHS. Στο σύνολο αυτό, υπολογίζεται αναλυτικά η ποσότητα ενδιαφέροντος J, με αποτέλεσμα και με τη βοήθεια της εξίσωσης 2.1 να προκύψει το γραμμικό σύστημα:

$$\mathbf{H}\ \vec{\alpha} = \vec{J} \tag{2.3}$$

Το σύστημα 2.3 είναι υπερκαθορισμένο, καθώς το πλήθος των δειγμάτων N είναι μεγαλύτερο του πλήθους των αγνώστων Q. Η λύση του συστήματος επιτυγχάνεται με χρήση ελαχίστων τετραγώνων (Least Squares). Η ορθολανονική βάση για κάθε αβέβαιη μεταβλητή επιλέγεται σύμφωνα με την κατανομή της: Hermite (Normal), Legendre (Uniform) κ.λπ.

Η μέση τιμή και η τυπική απόκλιση της ποσότητας ενδιαφέροντος υπολογίζονται από τις σχέσεις:

$$\mu_J = \alpha_0, \quad \sigma_J^2 \approx \sum_{i=1}^{Q-1} \alpha_i^2 \langle H_i(\vec{c})^2 \rangle \tag{2.4}$$

2.1.2 Γραμμική Παλινδρόμηση με χρήση παραγώγων

Η ενσωμάτωση πληροφοριών ευαισθησίας των ποσοτήτων ενδιαφέροντος ως προς τηςς αβέβαιες μεταβλητές στο σύστημα 2.3 οδηγεί σε δραστική μείωση του απαιτούμενου αριθμού δειγμάτων. Για κάθε δείγμα, πλέον οι πληροφορίες που συμμετέχουν στο σύστημα είναι:

$$[J(c), \ \frac{\partial J}{\partial c_1}, \ldots, \frac{\partial J}{\partial c_M}] \tag{2.5}$$

Προφανώς, όσο περισσότερες είναι οι αβέβαιες μεταβλητές, τόσο περισσότερες είναι και οι πληροφορίες που λαμβάνονται. Μάλιστα, με τεχνικές όπως η συζυγής μέθοδος, το σύνολο όλων των παραγώγων μπορεί να υπολογιστεί με κόστος ανάλογο αυτού της επίλυσης του πρωτεύοντος συστήματος. Επομένως, ανεξάρτητα από το πλήθος των αβέβαιων μεταβλητών, το κόστος υπολογισμού για κάθε δείγμα προσεγγίζεται ίσο με το διπλάσιο του κόστους υπολογισμού της ποσότητας ενδιαφέροντος.

2.2 Αυθαίρετο PCE (aPCE)

Το aPCE επιτρέπει επέκταση της παραπάνω θεωρίας για μη-τυπικές κατανομές, κατασκευάζοντας ορθοκανονική πολυωνυμική βάση προσαρμοσμένη στην εκάστοτε κατανομή της αβέβαιης μεταβλητής.

Η πολυωνυμική βάση $P^{(k)}(\xi) = \sum_{i=0}^{k} p_i^{(k)} \xi^i$ προκύπτει από το μητρώο Hankel M που εξαρτάται αμιγώς από τις στοχαστικές ροπές του δείγματος της μεταβλητής (βλ. Πλήρες Κείμενο). Μετά τη παραγοντοποίηση του M με τη μέθοδο Cholesky, $M = R^T R$, οι συντελεστές της βάσης αποτελούν τα μη μηδενικά στοιχεία του άνω τριγωνικού μητρώου R^{-1}.

Μετά την κατασκευή της βάσης, οι συντελεστές του αναπύγματος μπορούν να υπολογιστούν είτε με γραμμική παλινδρόμηση, όπως παρουσιάστηκε στην ενότητα 2, είτε αναλυτικά με προβολή της ποσότητας ενδιαφέροντος στην πολυωνυμική βάση. Στη περίπτωση αυτή, τα απαιτούμενα δείγματα υπολογίζονται από τη σχέση $Q = (1+k)^M$, ενώ τα σημεία δειγματοληψίας (Collocation Points ή GQ nodes) ταυτίζονται με τις ιδιοτιμές του Ιακωβιανού μητρώου του πίνακα M. Τέλος, τα αντίστοιχα βάρη ολοκλήρωσης για κάθε τέτοιο σημείο εξαρτώνται αμιγώ από τα ιδιοδιανύσματα του Ιακωβιανού πίνακα καθώς και από τις στοχαστικές ροπές του δείγματος (βλ. Πλήρες Κείμενο).

Κεφάλαιο 3

Ανάπτυγμα Karhunen-Loève

Το κεφάλαιο αυτό παρουσιάζει συνοπτικά το μαθηματικό πλαίσιο του ανάπτυγματος Karhunen-Loève (KL) για τη μοντελοποίηση γεωμετρικών ατελειών. Το ανάπτυγμα KL αποσυνθέτει μια τυχαία διαδικασία $w(x, \theta)$ σε μια σειρά ορθογώνικών ιδιοδιανυσμάτων:

$$w(x, \theta) = \bar{w}(x) + \sum_{n=0}^{\infty} \xi_n(\theta) \sqrt{\lambda_n} f_n(x), \tag{3.1}$$

όπου τα $\{\xi_n(\theta)\}$ είναι τυχαίες μεταβλητές που πρέπει να προσδιοριστούν, τα λ_n είναι σταθερές, και οι $\{f_n(x)\}$ είναι ορθοκανονικές ντετερμινιστικές συναρτήσεις. Επίσης, η $\bar{w}(x)$ εκφράζει την μέση τιμή όλων των πραγματοποιήσεων της διαδικασίας. Τα λ_n και $f_n(x)$ αποτελούν τις ιδιοτιμές και τις ιδιοσυναρτήσεις της συνάρτησης συσχέτισης $C(x_1, x_2)$ και προκύπτουν από την επίλυση της εξίσωσης 3.2.

$$\int_D C(x_1, x_2) f_n(x_2)\, dx_2 = \lambda_n f_n(x_1). \tag{3.2}$$

Η σειρά της εξίσωσης 3.2 αποκόπτεται στους πρώτους M όρους, με αποτέλεσμα να προκύπτουν και M αβέβαιες μεταβλητές, τα ξ_n. Η συνάρτηση συσχέτιση που χρησιμοποιείται στη παρούσα διπλωματική εργασία για τη μοντελοποίηση γεωμετρικών ατελειών σε αεροτομή, είναι η εκθετική: $C(s_1, s_2) = \sigma^2 e^{-|s_1 - s_2|/l}$, με $l = s_{\max}$ το μήκος συσχέτισης. Οι ιδιοσυναρτήσεις $f_n(s)$ προκύπτουν από τη λύση της διαφορικής εξίσωσης:

$$f''(s) + \omega^2 f(s) = 0, \tag{3.3}$$

Κεφάλαιο 4

Εφαρμογές στη Ποσοτικοποίηση Αβεβαιότητας

Στο πλαίσιο της διπλωματικής εργασίας, επιλέχθηκαν τρεις περιπτώσεις μελέτης προκειμένου να αξιολογηθεί η αποτελεσματικότητα των μεθόδων ποσοτικοποίησης αβεβαιότητας που αναπτύχθηκαν. Κάθε περίπτωση αντιπροσωπεύει ένα μοναδικό σενάριο αβεβαιότητας σε προβλήματα αεροδυναμικής, με στόχο τη συστηματική σύγκριση μεταξύ των κλασικών μεθόδων Πολυωνυμικού Αναπτύγματος Χάους και των παραλλαγών τους.

Η πρώτη περίπτωση μελέτης εστιάζει σε αβεβαιότητες των συνθηκών ροής γύρω από μια αεροτομή NACA 4415. Συγκεκριμένα, εξετάζονται αβεβαιότητες στην επ΄άπειρο ταχύτητα ροής, η οποία ακολουθεί κανονική κατανομή με μέση τιμή 240 μ/ς και τυπική απόκλιση 0.33 μ/ς, καθώς και στη γωνία πρόσπτωσης που ακολουθεί Beta κατανομή με όρια μεταξύ 1.6° και 2.5°. Το αεροδυναμικό μοντέλο βασίζεται στις εξισώσεις Euler, ενώ οι ποσότητες ενδιαφέροντος περιλαμβάνουν την άνωση και την οπισθέλκουσα.

Η δεύτερη περίπτωση εισάγει μια πιο πολύπλοκη πηγή αβεβαιότητας, μελετώντας γεωμετρικές ατελείες σε μια αεροτομή n16103 που προκύπτουν κατά την κατασκευή. Οι αβεβαιότητες μοντελοποιούνται μέσω της μεθόδου Karhunen-Loève, με 18 ανεξάρτητες τυχαίες μεταβλητές να περιγράφουν τις αποκλίσεις. Το μοντέλο βασίζεται στις εξισώσεις RANS με το μοντέλο τύρβης Spalart-Allmaras.

Η τρίτη περίπτωση αφορά την ποσοτικοποίηση αβεβαιότητας σε σχεδιαστικές παραμέτρους ενός υπερηχητικού επιχειρηματικού αεροσκάφους (SBJ). Δώδεκα κανονικά κατανεμημένες μεταβλητές περιγράφουν πτυχές όπως η επιφάνεια πτέρυγας, οι γωνίες σάρωσης, και το βάρος καυσίμου. Οι μετρικές απόδοσης περιλαμβάνουν την εμβέλεια, το μήκος απογείωσης και την ταχύτητα προσέγγισης.

Για κάθε περίπτωση μελέτης εφαρμόστηκαν τρεις προσεγγίσεις: αρχικά μια μέθοδος αναφοράς (είτε MCS είτε GQ-PCE), στη συνέχεια η μέθοδος γραμμικής παλινδρόμησης (regression-based PCE), και τέλος η εκδοχή με χρήση πληροφορίας παραγώγων μέσω αδθοιντ ή πεπερασμένων διαφορών.

Οι επιδόσεις αξιολογούνται ως προς ακρίβεια (σχετικό σφάλμα) και υπολογιστικό κόστος (Equivalent Flow Solutions - EFS). Τα πλήρη αποτελέσματα συνοψίζονται στον εκτενή Πίνακα 4.1.

Μέθοδος	**Ποσότητα Ενδιαφέροντος**	**Μέση Τιμή**	**Σφάλμα MT (%)**	**Τυπική Απόκλιση**	**Σφάλμα ΤΑ (%)**	**Κόστος**
Περίπτωση Μελέτης 1: NACA 4415 (2 αβέβαιες μεταβλητές)						
GQ-PCE	Άνωση	336.54131	-	8.40852	-	9
GQ-PCE	Οπισθέλκουσα	20.21745	-	1.42208	-	9
Reg-PCE (order 2)	Άνωση	336.55	0.0025	8.41011	0.0189	15
Reg-PCE (order 2)	Οπισθέλκουσα	20.2197	0.0111	1.42251	0.0304	15
Adjoint-Reg-PCE	Άνωση	336.55	0.003	8.411	0.03	4
Adjoint-Reg-PCE	Οπισθέλκουσα	20.22	0.0126	1.4282	0.0523	4
Περίπτωση Μελέτης 2: n16103 (18 αβέβαιες μεταβλητές)						
Reg-PCE	Άνωση	2,262.2	-	93.52	-	600
Reg-PCE	Οπισθέλκουσα	46.58	-	1.07	-	600
Adjoint-PCE (50 δείγματα)	Άνωση	2,263.5	0.06	91.4	-2.27	100
Adjoint-PCE (50 δείγματα)	Οπισθέλκουσα	46.52	-0.13	1.10	2.80	100
Adjoint-PCE (30 δείγματα)	Άνωση	2,264.7	0.11	89.1	-4.73	60
Adjoint-PCE (30 δείγματα)	Οπισθέλκουσα	46.45	-0.28	1.13	5.60	60
Περίπτωση Μελέτης 3: SBJ (12 αβέβαιες μεταβλητές)						
MCS	Εμβέλεια	2,786.6	-	392.1	-	10^8
MCS	Απογείωση	4,154.8	-	546.3	-	10^8
MCS	Προσέγγιση	87.477	-	3.852	-	10^8
Reg-PCE	Εμβέλεια	2,777.8	-0.31	402.6	2.67	182
Reg-PCE	Απογείωση	4,149.2	-0.13	547.2	0.16	182
Reg-PCE	Προσέγγιση	87.491	0.02	3.853	-0.04	182
Grad-Reg-PCE	Εμβέλεια	2,775.6	-0.39	399.3	1.85	28
Grad-Reg-PCE	Απογείωση	4,148.2	-0.16	544.2	-0.38	28
Grad-Reg-PCE	Προσέγγιση	87.498	0.02	3.873	0.56	28

Πίνακας 4.1: *Αποτελέσματα περιπτώσεων μελέτης ποσοτικοποίησης αβεβαιότητας.*

Όπως φαίνεται από τον Πίνακα 4.1, η μέθοδος Adjoint-assisted PCE παρέχει καλή ακρίβεια ακόμα και με ελάχιστα δείγματα. Είναι ιδιαίτερα χρήσιμη σε προβλήματα υψηλής διάστασης, καθώς μειώνει δραστικά τα απαιτούμενα δείγματα ενσωματώνοντας πληροφορίες ευαισθησίας ως προς όλες τις αβέβαιες μεταβλητές, επιτρέποντας την αποδοτική ενσωμάτωση της αβεβαιότητας στον αεροδυναμικό σχεδιασμό.

Βιβλιογραφία

[1] Eldred, M.S.: Recent advances in non-intrusive polynomial chaos and stochastic collocation methods for uncertainty analysis and design. American Institute of Aeronautics and Astronautics Paper (2009–2274) (2009)

[2] Marelli, S., Sudret, B.: Uqlab user manual - polynomial chaos expansions. Tech. rep., Chair of Risk, Safety & Uncertainty Quantification, ETH Zurich (2015)

[3] Oladyshkin, S., Nowak, W.: Data-driven uncertainty quantification using the arbitrary polynomial chaos expansion. Reliability Engineering and System Safety **106**, 179–190 (2012). https://doi.org/10.1016/j.ress.2012.05.002, http://www.elsevier.com/locate/ress

[4] Papoutsis-Kiachagias, E., Asouti, V., Giannakoglou, K.: Assessment of variants of the method of moments and polynomial chaos approaches to aerodynamic uncertainty quantification. Uncertainty Quantification in Computational Sciences and Engineering **4**(1), 1–20 (Jun 2021)

[5] Saracco, P., Batic, M., Hoff, G., Pia, M.G.: Uncertainty quantification (uq) in generic montecarlo simulations. IEEE Transactions on Nuclear Science pp. 2805–2813 (2012)